

Augmented Skew-Symmetric System for Shallow-Water System with Surface Tension Allowing Large Gradient of Density

D. Bresch, N. Cellier, F. Couderc, M. Gisclon,
P. Noble, G.-L. Richard, C. Ruyer-Quil, J.-P. Vila

June 11, 2020

Abstract

In this paper, we introduce a new extended version of the shallow-water equations with surface tension which may be decomposed into a hyperbolic part and a second order derivative part which is skew-symmetric with respect to the L^2 scalar product. This reformulation allows for large gradients of fluid height simulations using a splitting method. This result is a generalization of the results published by P. Noble and J.-P. Vila in [*SIAM J. Num. Anal.* (2016)] and by D. Bresch, F. Couderc, P. Noble and J.P. Vila in [*C.R. Acad. Sciences Paris* (2016)] which are restricted to quadratic forms of the capillary energy respectively in the one dimensional and two dimensional setting. This is also an improvement of the results by J. Lallement, P. Villedieu *et al.* published in [AIAA Aviation Forum 2018] where the augmented version is not skew-symmetric with respect to the L^2 scalar product. Based on this new formulation, we propose a new numerical scheme and perform a nonlinear stability analysis. Various numerical simulations of the shallow water equations are presented to show differences between quadratic (w.r.t the gradient of the height) and general surface tension energy when high gradients of the fluid height occur.

1 Introduction

In this paper, we consider compressible Euler type equations with capillarity (such as the shallow-water system with surface tension), in the two-dimensional setting, issued from Hamiltonian formulation in the spirit of P. Casal and H. Gouin ([6]) (see also D. Serre ([29])). There exists a large body of literature on various numerical techniques for simulating the shallow-water equations without capillarity terms for a variety of applications, such as discontinuous Galerkin methods (e.g., Giraldo [13], Giraldo et al. [15], Eskilsson and Sherwin [10], Nair et al. [26], Xing et al. [30], Blaise and St-Cyr [2]), in addition to spectral methods (e.g., Giraldo and Warburton [16], Giraldo [14]), and purely Lagrangian approaches (e.g., Frank and Reich [11], Capecelatro [7]). When dispersive effect is included, everything change and numerous attempts have been conducted to try to get rid spurious currents (also known as parasitic currents) generated at the free surface due to the presence of the third-order term coming from the capillarity quantity. Augmented versions have been proposed to decrease the level of derivative in the system but with not enough properties to allow to design an efficient numerical method to compute for instance large gradient of density. This is the objective of our paper to propose an appropriate extended formulation which allows an appropriate splitting method. To be more precise, let us define the internal energy E as follows

$$E(h, \mathbf{p}) = \Phi(h) + \sigma(h) \mathcal{E}_{\text{cap}}(\|\mathbf{p}\|) \quad (1)$$

with h the density of the fluid (or the fluid height if we consider the shallow-water system), $\mathbf{p} = \nabla h$ and $\Phi(h)$ the pressure contribution and $\sigma(h)\mathcal{E}_{\text{cap}}(\|\mathbf{p}\|)$ the capillarity energy (Note that $s \mapsto \Phi(s)$, $s \mapsto \sigma(s)$ and $s \mapsto \mathcal{E}_{\text{cap}}(s)$ are three given positive scalar functions). We consider the following system

$$\begin{cases} \partial_t h + \text{div}(h\mathbf{u}) = 0 & (i) \\ \partial_t(h\mathbf{u}) + \text{div}(h\mathbf{u} \otimes \mathbf{u}) + \nabla P = -\text{div}(\nabla h \otimes \nabla_{\mathbf{p}} E) + \nabla(h \text{div}(\nabla_{\mathbf{p}} E)) & (ii) \end{cases} \quad (2)$$

which is obtained as the Euler-Lagrange equation related to the total energy (sum of the kinetic $h|\mathbf{u}|^2/2$ and internal energy $E(h, \mathbf{p})$ given by (1)) under the conservation of mass constraint with \mathbf{u} the fluid velocity vector field and P the pressure law given by

$$P(h, \mathbf{p}) := h \partial_h E(h, \mathbf{p}) - E(h, \mathbf{p}) = \pi(h) - (\sigma(h) - h\sigma'(h)) \mathcal{E}_{\text{cap}}(\|\mathbf{p}\|), \quad (3)$$

where

$$\frac{\pi(h)}{h^2} = \left(\frac{\Phi(s)}{s} \right)' \Big|_{s=h}. \quad (4)$$

In all the paper long, we will do the following hypothesis:

- $s \mapsto \mathcal{E}_{\text{cap}}(s)$, $s \mapsto \Phi(s)$ and $s \mapsto \sigma(s)$ are assumed to be positive,
- \mathcal{E}_{cap} invertible from \mathbb{R}^+ to \mathbb{R}^+ with $\mathcal{E}_{\text{cap}}(0) = 0$,
- $\pi'(h) > 0$ so that Φ is strictly convex as soon as $h > 0$.

System (1)–(4) is supplemented with the initial data

$$h|_{t=0} = h_0, \quad h\mathbf{u}|_{t=0} = m_0. \quad (5)$$

In this context, System (1)–(5) admits an additional energy conservation law which reads

$$\partial_t \left(\frac{1}{2} h \|\mathbf{u}\|^2 + E \right) + \text{div} \left(\left(\frac{1}{2} h \|\mathbf{u}\|^2 + E + P \right) \mathbf{u} \right) - \text{div} (\text{div} (\nabla_{\mathbf{p}} E) h \mathbf{u}) + \text{div} (\text{div} (h \mathbf{u}) \nabla_{\mathbf{p}} E) = 0. \quad (6)$$

Remark. For specific choices of the capillary energy, we note that the system (2) reduces to classical models of the fluid mechanics literature like

- The Euler-Korteweg isothermal system when :

$$E(h, \nabla h) = \Phi(h) + \frac{1}{2} \sigma(h) \|\nabla h\|^2$$

where h is the density and $\sigma(h)$ is the capillary coefficient.

- The shallow-water type system for thin film flows both:
- In the quadratic capillary case

$$E(h, \nabla h) = \frac{h^2}{2} + \frac{1}{2} \sigma \|\nabla h\|^2 \text{ with } h \text{ the height of the fluid and } \sigma \text{ is constant}$$

- In the fully nonlinear capillary case :

$$E(h, \nabla h) = \frac{h^2}{2} + \sigma \sqrt{1 - \|\nabla h\|^2} \text{ with } h \text{ the height of the fluid and } \sigma \text{ is constant}$$

Note that the fully nonlinear case admits the following two asymptotics

$$E(h, \nabla h) = h^2/2 + \sigma \|\nabla h\|^2/2 + o_{\|\nabla h\| \rightarrow 0} (\|\nabla h\|)$$

and

$$E(h, \nabla h) = h^2/2 + \sigma \|\nabla h\| + o_{\|\nabla h\| \rightarrow \infty} (\|\nabla h\|)$$

It is a hard problem to propose a discretization of System (1)–(5) that is compatible with the energy equation (6) and this is the objective of our paper. The main issue is that one cannot adapt the proof of the energy estimate (6) derived from (2) at a discretized level due to the presence of high-order derivatives associated to the capillarity energy (1). The readers interested in understanding the mathematical and numerical difficulties are referred to [25] and important references cited therein. The strategy first consists in performing a reduction of order in spatial derivatives and in introducing an alternative system (called augmented system) which contains lower order derivatives. It consists secondly in checking that the augmented system may be decomposed into two parts: A conservative hyperbolic part and a second order derivatives part which is skew-symmetric with respect to the L^2 scalar product. Such system is really adapted to discretization compatible with the energy: it is obtained by taking L^2 scalar products with respect to the new unknowns. This strategy was applied successfully in the context of Euler-Korteweg isothermal system for numerical purposes when the internal energy is quadratic with respect to ∇h : see [24] in the one dimensional case and [3] in the two dimensional case. In both cases, the augmented version is obtained by introducing an auxiliary velocity \mathbf{v} which is proportional to ∇h and admits an additional skew-symmetric structure with respect to the L^2 scalar product which makes the proof of energy estimates and the design of compatible numerical scheme easier. However, this approach was not extended to more general internal energy (1). This is the objective of the paper to define the appropriate unknowns in order to get an appropriate augmented system for numerical purposes.

Note that there exists several interesting papers developing augmented systems such as [12] and [17] for symmetric form for capillarity fluids with a capillarity energy $E(h, \nabla h)$ or multi-gradient fluids with a capillarity energy $E(h, \nabla h, \dots, \nabla^n h)$. See also recently [8] for the defocusing Schrödinger equation which is linked to the quantum-Euler system ($E(h, \mathbf{p}) = \Phi(h) + \sigma \|\mathbf{p}\|^2/h$ where σ is constant) through the Madelung transform and some numerical simulation.

It is interesting to note that the augmented system in [12] and [17] is related to the unknowns $(h, \mathbf{u}, \nabla h, \dots, \nabla^n h)$. In [21], the authors developed a similar augmented version in order to deal with internal capillarity energies (1) for numerical purposes namely:

$$\begin{cases} \partial_t h + \operatorname{div}(h\mathbf{u}) = 0 & (i) \\ \partial_t(h\mathbf{u}) + \operatorname{div}(h\mathbf{u} \otimes \mathbf{u}) + \nabla P + \operatorname{div}(\mathbf{p} \otimes \nabla_{\mathbf{p}} E_{tot}) = \nabla(h \operatorname{div}(\nabla_{\mathbf{p}} E_{tot})) & (ii) \\ \partial_t \mathbf{p} + \nabla(\mathbf{p}^t \mathbf{u}) = -\nabla(h \operatorname{div}(\mathbf{u})) & (iii) \end{cases} \quad (7)$$

where $E_{tot} = h|\mathbf{u}|^2/2 + E(h, \mathbf{p})$. However, in the 2-dimensional setting, the assumption $\operatorname{curl} \mathbf{p} = 0$ has to be made to show the conservation of the total energy and therefore it has to be satisfied initially: The interested reader is referred pages 166–168. This constraint is not satisfied at the discretized level and it creates instabilities.

Remark. In order to avoid such a constraint which is hardly guaranteed in the discrete case, one could use instead the following modified formulation

$$\begin{cases} \partial_t h + \operatorname{div}(h\mathbf{u}) = 0 & (i) \\ \partial_t(h\mathbf{u}) + \operatorname{div}(h\mathbf{u} \otimes \mathbf{u}) + \nabla P + \operatorname{div}(\mathbf{p} \otimes \nabla_{\mathbf{p}} E_{tot}) - \left((\nabla \mathbf{p})^t - (\nabla \mathbf{p}) \right) \nabla_{\mathbf{p}} E_{tot} = \nabla(h \operatorname{div}(\nabla_{\mathbf{p}} E_{tot})) & (ii) \\ \partial_t \mathbf{p} + \nabla(\mathbf{p}^t \mathbf{u}) = -\nabla(h \operatorname{div}(\mathbf{u})) & (iii) \end{cases}$$

for which it is easy to prove the conservation of the total energy

$$\begin{aligned} \partial_t(E_{tot}) + \operatorname{div}(\mathbf{u}(E_{tot} + \pi)) &= (\operatorname{div}(h(\mathbf{u}^t \nabla)(\nabla_{\mathbf{p}} E_{tot})) - \operatorname{div}(h(\nabla_{\mathbf{p}} E_{tot}^t \nabla)\mathbf{u})) \\ &\quad - \operatorname{div}(\mathbf{u}(\mathbf{p}^t \nabla_{\mathbf{p}} E_{tot} - (\sigma - h\sigma') \mathcal{E}_{cap})) \end{aligned}$$

for any smooth solution of the above system without assuming the curl free assumption on \mathbf{p} . However, this formulation introduces non-conservative terms in the left-hand side of the momentum equation and it is then hard to satisfy for conservation of momentum and energy at the discrete level.

In our paper, defining an appropriate velocity field \mathbf{v} instead of \mathbf{p} , we are able to design an appropriate augmented version which may be decomposed as the sum of a conservative hyperbolic part and a skew-symmetric second order differential operator for the L^2 scalar product. The system is solved in the variables $(h, \mathbf{u}, \mathbf{v})$ and if regularity occurs we recover the expression of \mathbf{v} in terms of h, \mathbf{p} and $\|\mathbf{p}\|$. The important

property is that the energy conservation law may be satisfied easily at the discretized level using the particular structure of our augmented system. The particular form allows also an efficient splitting method allowing to simulate complex situations like large gradients of fluid height.

In the small gradient limit, this formulation is equivalent to the one derived by D. Bresch, F. Couderc, P. Noble and J.-P. Vila in [3]. Our formulation is valid for any internal energy in the form $E(h, \mathbf{p}) = \Phi(h) + \sigma(h)\mathcal{E}_{cap}(\|\mathbf{p}\|)$. When specified to $\mathcal{E}_{cap}(q) = \sqrt{1+q^2} - 1$, we see that in the high gradient limit, $\mathcal{E}_{cap}(q) \sim_{q \rightarrow \infty} |q|$ which is a capillary term found usually in two fluids systems. We thus expect our approach to be useful in the context of bi-fluid flows. Note also that our paper could be also of practical interest to deal with generalization of Euler-Korteweg system: see [20] and [18] for discussions on compressible Korteweg type systems.

We rely on the new augmented system to propose a numerical scheme which is energetically stable and extends what was done in [3] and [24]. Note that skew-symmetric augmented versions of the capillary shallow water equations in the L^2 scalar product are also useful from a theoretical point of view: see e.g. [5] for the proof of existence of dissipative solutions to the Euler-Korteweg isothermal system. Our present work will be the starting point to improve the work by Lallement and Villedieu (see [21] and [22]) related to disjunction term for triple point simulations: see [4].

The paper is divided in three parts: The first part introduces the augmented version with full surface tension and discuss its connection with the system derived in [3]. In the second part, we propose a numerical scheme satisfying energy stability. Finally, we present numerical illustrations based on our numerical scheme showing the importance of considering our augmented system with the full surface tension.

2 Augmented version

Extending ideas from [24] in the one dimensional case, an augmented formulation of the shallow water equations (2) with $\mathcal{E}_{cap}(\|\nabla h\|) = \frac{\sigma}{2} \|\nabla h\|^2$ was proposed in [3] in the two dimensional setting: it is a second order system of PDEs which may be decomposed in two parts: A conservative hyperbolic part and a second order derivatives part which is skew symmetric with respect to the L^2 scalar product. The additional quantity in [3] was given by $\mathbf{w} = \nabla\phi(h)$ with $\phi'(h) = \sqrt{\sigma(h)/h}$: it is thus colinear to ∇h .

The main objective here is to consider a more general internal capillarity energy namely (1). We now introduce our new formulation of (2) which is valid in the fully decoupled case and provides a dual formulation of capillary terms which ensures a straightforward consistent energy balance. To this end we introduce an additional unknown, denoted \mathbf{v} , which is colinear to ∇h and satisfies

$$\frac{1}{2}h \|\mathbf{v}\|^2 = \sigma(h) \mathcal{E}_{cap}(\|\nabla h\|)$$

where $q = \|\mathbf{p}\| = \|\nabla h\|$. To do so, we define \mathbf{v} as

$$\mathbf{v} = \alpha(q^2) \sqrt{\frac{\sigma(h)}{h}} \mathbf{p} \tag{8}$$

where the function $\alpha : s \mapsto \alpha(s)$ is given by

$$\alpha(s) = \sqrt{\frac{2\mathcal{E}_{cap}(\sqrt{s})}{s}}.$$

Remark. Note that using the definition \mathbf{v} , we have the following relations

$$\|\mathbf{v}\|^2 = \alpha^2(\|\mathbf{p}\|^2) \|\mathbf{p}\|^2 \frac{\sigma}{h},$$

$$\frac{1}{2}\alpha^2(q^2) q^2 \sigma(h) = \sigma(h)\mathcal{E}_{cap}(q).$$

Remark. Note that \mathbf{v} has the dimension of a velocity and transforms the capillary energy into some kinetic energy. This interpretation of the capillary energy in terms of kinetic energy in our augmented system defined below motivates surely the robustness of our results.

Let us now write a system related to the unknowns $(h, \mathbf{u}, \mathbf{v})$ where \mathbf{v} is given by (8) with $\mathbf{p} = \nabla h$. This will provide a system which combines a first order conservative and hyperbolic part on $(h, \mathbf{u}, \mathbf{v})$ together with a second order part which has a skew-symmetric structure (for the L^2 scalar product). More precisely, we have the following result.

Lemma 2.1 *i) Let*

$$\mathbf{U} = \begin{pmatrix} h \\ h\mathbf{u} \\ h\mathbf{v} \end{pmatrix}, \quad \mathcal{F}(\mathbf{U}) = \begin{pmatrix} h\mathbf{u} \\ h\mathbf{u} \otimes \mathbf{u} + \pi(h)\mathbf{I}_d \\ h\mathbf{v} \otimes \mathbf{u} \end{pmatrix} \quad (9)$$

where \mathbf{I}_d is the $d \times d$ identity matrix and

$$\mathbf{M} = \mathcal{M}(h, \mathbf{v})(\mathbf{U})$$

with, for all $\mathbf{U}_1 = (h_1, h_1\mathbf{u}_1, h_1\mathbf{v}_1)^t$,

$$\mathcal{M}(h, \mathbf{v})(\mathbf{U}_1) = \begin{pmatrix} 0 \\ \operatorname{div}(h\nabla(f(h, \mathbf{v})\mathbf{v}_1)^t) - \nabla(\mathbf{g}(h, \mathbf{v})^t\mathbf{v}_1) \\ -f(h, \mathbf{v})\operatorname{div}(h\nabla\mathbf{u}_1^t) - \mathbf{g}(h, \mathbf{v})\operatorname{div}\mathbf{u}_1 \end{pmatrix} \quad (10)$$

where $f(h, \mathbf{v})$ is a symmetric tensor and $\mathbf{g}(h, \mathbf{v})$ a vector field given by

$$f(h, \mathbf{v}) = \sqrt{\sigma(h)}\sqrt{h} \left(2\frac{\alpha'(q^2)h}{\alpha(q^2)^2\sigma(h)}\mathbf{v} \otimes \mathbf{v} + \alpha(q^2)\mathbf{I}_d \right)$$

$$\mathbf{g}(h, \mathbf{v}) = \left(\left(\frac{\sigma'(h)h}{2\sigma(h)} + \frac{1}{2} \right) + 2\frac{\alpha'(q^2)}{\alpha(q^2)}q^2 \right) h\mathbf{v}$$

and

$$\alpha(q^2) = \frac{\sqrt{2\mathcal{E}_{\text{cap}}(q)}}{q} \quad \text{with} \quad q = \mathcal{E}_{\text{cap}}^{-1} \left(\frac{h\|\mathbf{v}\|^2}{2\sigma(h)} \right).$$

The augmented system reads

$$\partial_t \mathbf{U} + \operatorname{div}(\mathcal{F}(\mathbf{U})) = \mathbf{M}. \quad (11)$$

ii) If $(h, \mathbf{u}, \mathbf{v})$ is regular enough then it also satisfies the following energy balance

$$\begin{aligned} \partial_t \left(\frac{1}{2}h\|\mathbf{u}\|^2 + E \right) &+ \operatorname{div} \left(\mathbf{u} \left(\frac{1}{2}h\|\mathbf{u}\|^2 + E + \pi \right) \right) \\ &= (\operatorname{div}(h\mathbf{u}^t\nabla^t(f(h, \mathbf{v})^t\mathbf{v})) - \operatorname{div}(h\nabla\mathbf{u}f(h, \mathbf{v})\mathbf{v})) - \operatorname{div}(\mathbf{u}(f(h, \mathbf{v})^t\mathbf{v})) \end{aligned} \quad (12)$$

where $E = \Phi(h) + h\|\mathbf{v}\|^2/2$.

iii) If (h, \mathbf{u}) is regular enough and the initial velocity \mathbf{v}_0 satisfies

$$\mathbf{v}_0 = \alpha(\|\nabla h_0\|^2) \sqrt{\frac{\sigma(h_0)}{h_0}} \nabla h_0$$

then \mathbf{v} satisfies also

$$\mathbf{v} = \alpha(\|\nabla h\|^2) \sqrt{\frac{\sigma(h)}{h}} \nabla h$$

and (h, \mathbf{u}) solves the original equations with the full surface tension term given by (2)–(3).

3 Energetically stable numerical scheme

The augmented formulation (11) in Lemma 2.1 reads

$$\partial_t \mathbf{U} + \operatorname{div}(\mathcal{F}(\mathbf{U})) = \mathbf{M}$$

with definitions (9) and (10) of \mathbf{U} , \mathcal{F} and \mathbf{M} . The first order part of the augmented formulation in the left-hand side is the classical Euler barotropic model with an additional transport equation. It admits an additional conservation law related to the total energy:

$$E_{tot} = \frac{\|h\mathbf{u}\|^2}{2h} + \Phi(h) + \frac{\|h\mathbf{v}\|^2}{2h}.$$

whereas the entropy variable is

$$(\nabla_{\mathbf{U}} E_{tot})^t = \mathbf{V}^t = \left(-\frac{1}{2} (\|\mathbf{u}\|^2 + \|\mathbf{v}\|^2) + \Phi'(h), \mathbf{u}^t, \mathbf{v}^t \right).$$

This total energy is the total energy of the shallow-water equations with surface tension whereas the potential energy associated to surface tension is transformed into kinetic energy associated to the artificial velocity \mathbf{v} . The full system admits also an energy equation:

$$\begin{aligned} \partial_t E_{tot} + \operatorname{div}(\mathbf{u}(E_{tot} + \pi(h))) &= \mathbf{V}^t \mathbf{M} \\ &= \operatorname{div}(h\mathbf{u}^t \nabla(\nabla_{\mathbf{p}} E)) - \operatorname{div}(h(\nabla_{\mathbf{p}} E)^t \nabla \mathbf{u}) \\ &\quad - \operatorname{div}(\mathbf{u}(\mathbf{p}^t \nabla_{\mathbf{p}} E - (\sigma - h\sigma') \mathcal{E}_{\text{cap}}(q))) \end{aligned}$$

with the right-hand side in conservation form. One of the aim of this paper is to design a numerical scheme that is free from a CFL condition associated to surface tension. For that purpose, we follow the strategy in [3] and introduce an IMplicit-EXplicit strategy where the hyperbolic step is explicit in time whereas the step associated to surface tension is implicit in time. The spatial discretization is based on an entropy dissipative scheme for the first order part whereas we mimic the skew symmetric structure found at the continuous level to discretize the right hand side \mathcal{M} . We prove that this strategy is energetically stable in the case of periodic boundary conditions.

3.1 IMplicit - EXplicit formulation

Following [3], we consider the following IMplicit-EXplicit time discretization: the hyperbolic step is explicit

$$\frac{\mathbf{U}^{n+1/2} - \mathbf{U}^n}{\Delta t} + \operatorname{div}(\mathcal{F}(\mathbf{U}^n)) = 0 \tag{13}$$

and the capillary skew symmetric second order step

$$\frac{\mathbf{U}^{n+1} - \mathbf{U}^{n+1/2}}{\Delta t} = \mathbf{M}^{n+1} \tag{14}$$

with

$$\mathbf{M}^{n+1} = \begin{pmatrix} 0 \\ \operatorname{div}(h^{n+1} \nabla(f(h^{n+1}, \mathbf{v}^{n+1/2}) \mathbf{v}^{n+1})^t) - \nabla(g(h^{n+1}, \mathbf{v}^{n+1/2})^t \mathbf{v}^{n+1}) \\ -f(h^{n+1}, \mathbf{v}^{n+1/2}) \operatorname{div}(h^{n+1} \nabla(\mathbf{u}^{n+1})^t) - g(h^{n+1}, \mathbf{v}^{n+1/2}) \operatorname{div} \mathbf{u}^{n+1} \end{pmatrix}.$$

The second step is not fully implicit: instead it is semi-implicit so that the problem to solve for $(\mathbf{v}^{n+1}, \mathbf{u}^{n+1})$ is *linear*. This does not affect the order of the time discretization since the time splitting is already first order in time. Let us now consider the spatial discretization. We will use a generic Finite Volume context. We introduce a spatial discretization of ∇ and div operators with finite volume methods. For that purpose, we denote \mathbf{K} a cell of the mesh T_d , $\mathbf{e} \in \partial \mathbf{K}$ an edge of \mathbf{K} and \mathbf{K}_e a neighboring cell of \mathbf{K} : see figure 1 for an illustration. We use a classical entropy satisfying scheme of numerical flux

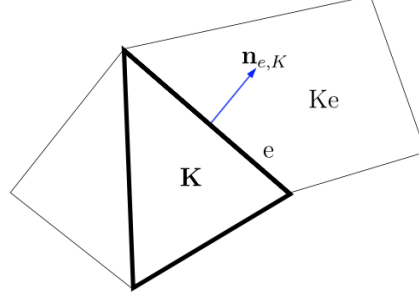


Figure 1: Notations for cell \mathbf{K}

$$\mathbf{G}_{e,K}^n = \mathbf{G}(\mathbf{U}_K^n, \mathbf{U}_{K_e}^n, n_{e,K})$$

where $n_{e,K}$ is the outward normal to the cell K (of measure m_K) at the edge e (of measure m_e). We denote \mathbf{U}_K the average of the vector \mathbf{U} on the cell \mathbf{K} . The hyperbolic step then reads

$$\mathbf{U}_K^{n+1/2} = \mathbf{U}_K^n - \frac{\Delta t}{m_K} \sum_{e \in \partial K} m_e \mathbf{G}_{e,K}^n \quad (15)$$

and we assume that it is entropy dissipative in the sense that it satisfies the following discrete Entropy inequality

$$E_{tot}(\mathbf{U}_K^{n+1/2}) \leq E_{tot}(\mathbf{U}_K^n) - \frac{\Delta t}{m_K} \sum_{e \in \partial K} m_e H_{e,K}^n \quad (16)$$

where $H_{e,K}^n$ is the entropy numerical flux associated with $G_{e,K}^n$. In the particular case of Euler Barotropic equations such numerical schemes exist and satisfy this inequality provided a hyperbolic CFL condition of the type

$$\max_K \frac{\Delta t}{m_K} m_e \|\nabla_{\mathbf{U}} F(\mathbf{U}_K^n)\| < a < 1 \quad (17)$$

is satisfied for some $a > 0$. Moreover, under a similar CFL condition, the positivity of the fluid h is preserved and the total energy $E_{tot}(\mathbf{U})$ is strictly convex: this will be a useful property to prove entropy stability for numerical schemes. The second step is

$$\mathbf{U}_K^{n+1} = \mathbf{U}_K^{n+1/2} + \Delta t \mathbf{M}_K^{n+1} \quad (18)$$

with

$$\mathbf{M}_K^{n+1} = \begin{pmatrix} 0 \\ -\nabla_{3,\Delta}(\mathbf{g}(h_K^{n+1}, \mathbf{v}_K^{n+1/2})^t \mathbf{v}_K^{n+1}) + \text{div}_{1,\Delta} \left(h_K^{n+1} \nabla_{1,\Delta} \left(f(h_K^{n+1}, \mathbf{v}_K^{n+1/2}) \mathbf{v}_K^{n+1} \right)^T \right) \\ -\mathbf{g}(h_K^{n+1}, \mathbf{v}_K^{n+1/2}) \text{div}_{3,\Delta}(\mathbf{u}_K^{n+1}) - f(h_K^{n+1}, \mathbf{v}_K^{n+1/2}) \text{div}_{1,\Delta} \left(h_K^{n+1} \nabla_{1,\Delta}(\mathbf{u}_K^{n+1})^T \right) \end{pmatrix} \quad (19)$$

where $\nabla_{3,\Delta}$, $\text{div}_{1,\Delta}$, $\nabla_{1,\Delta}^T$, $\text{div}_{3,\Delta}$ are linear discrete operators approximating the corresponding ones in the definition of the operator \mathcal{M} and that will be defined hereafter. In particular $\text{div}_{3,\Delta}$ shall be chosen as the dual discrete operator of $\nabla_{3,\Delta}$ in the following sense :

$$(a, \nabla_{3,\Delta}(\varphi))_{T_d} = -(\text{div}_{3,\Delta}(a), \varphi)_{T_d} \quad (20)$$

for any smooth function φ and a defined on the mesh T_d where we have used the discrete scalar product below

$$(a, b)_{T_d} = \sum_{K \in T_d} m_K \langle a_K, b_K \rangle_{\mathbb{R}^d}.$$

One possible choice is taking the classical approximation of flux in the finite volume context which leads to

$$\operatorname{div}_{3,\Delta}(\mathbf{a}) = \frac{1}{m_K} \sum_{e \in \partial K} m_e \frac{1}{2} (\mathbf{a}_{K_e} + \mathbf{a}_K) \cdot \mathbf{n}_{e,K} = \frac{1}{2m_K} \sum_{e \in \partial K} m_e \mathbf{a}_{K_e} \cdot \mathbf{n}_{e,K}$$

and the corresponding (weak) approximation of $\nabla_{3,\Delta}(\varphi)$

$$\nabla_{3,\Delta}(\varphi) = \frac{1}{2m_K} \sum_{e \in \partial K} m_e \frac{1}{2} \left(\varphi_K \frac{m_{K_e}}{m_K} - \varphi_{K_e} \right) \mathbf{n}_{e,K}.$$

In the context of finite difference approximations, we may consider the discrete analogues of the div operator

$$\operatorname{div}_{3,\Delta}(\mathbf{a})_{ij} = \frac{a_{i+1,j}^x - a_{i-1,j}^x}{2\Delta x} + \frac{a_{i,j+1}^y - a_{i,j-1}^y}{2\Delta y} \quad (21)$$

which leads to

$$\nabla_{3,\Delta}(\varphi)_{ij} = \frac{\varphi_{i+1,j} - \varphi_{i-1,j}}{2\Delta x} \mathbf{n}_x + \frac{\varphi_{i,j+1} - \varphi_{i,j-1}}{2\Delta y} \mathbf{n}_y. \quad (22)$$

Remark 3.1 *In the case of general finite volume discretization on any mesh, the question of finding consistent second order operators is not so simple and requires some refined tools such as renormalisation or adhoc discrete gradient (see eg [1, 23, 19]).*

In the next section, we focus on the definition of the discrete divergence and gradients operators $\operatorname{div}_{1,\Delta}$ and $\nabla_{1,\Delta}$ so as to ensure the energy stability.

3.2 Energy Stability of first order schemes

Let us now analyse the stability properties of the above scheme. The hyperbolic step is entropy stable in the sense that

$$\sum_K E_{tot}(\mathbf{U}_K^{n+1/2}) m_K \leq \sum_K E_{tot}(\mathbf{U}_K^n) m_K.$$

since it is a direct consequence of entropy inequality (16). Let us now focus on the ‘‘capillary time step’’ and the definition of $\operatorname{div}_{1,\Delta}$ and $\nabla_{1,\Delta}$. In order to get more compact form of discrete operators, let us define

$$\begin{aligned} (\partial_{x,1\Delta}(m))_{i+1/2,j} &= \frac{m_{i+1,j} - m_{i,j}}{\Delta x}, & (\partial_{x,1\Delta}^0(p))_{i,j} &= \frac{p_{i+1/2,j} - p_{i-1/2,j}}{\Delta x}, & (\partial_{x,1\Delta}^{00}(m))_{i,j} &= \frac{m_{i+1,j} - m_{i-1,j}}{2\Delta x}, \\ (\partial_{y,1\Delta}(m))_{i,j+1/2} &= \frac{m_{i,j+1} - m_{i,j}}{\Delta y}, & (\partial_{y,1\Delta}^0(p))_{i,j} &= \frac{p_{i,j+1/2} - p_{i,j-1/2}}{\Delta y}, & (\partial_{y,1\Delta}^{00}(m))_{i,j} &= \frac{m_{i,j+1} - m_{i,j-1}}{2\Delta y} \end{aligned} \quad (23)$$

$$\operatorname{div}_{1,\Delta}(h\nabla_{1,\Delta}\mathbf{m}^T) = \begin{pmatrix} (\partial_{x,1\Delta}^0(h\partial_{x,1\Delta}m^x)) + (\partial_{y,1\Delta}^{00}(h\partial_{x,1\Delta}^{00}m^y)) \\ (\partial_{x,1\Delta}^{00}(h\partial_{y,1\Delta}^{00}m^x)) + (\partial_{y,1\Delta}^0(h\partial_{y,1\Delta}m^y)) \end{pmatrix} \quad (24)$$

We thus have the following property :

Lemma 3.2 *Let us suppose that $\operatorname{div}_{1,\Delta}(h\nabla_{1,\Delta}\mathbf{m}^T)$ is defined as (24): Then we have*

$$(\mathbf{u}, \operatorname{div}_{1,\Delta}(h\nabla_{1,\Delta}\mathbf{m}^T))_{T_d} = (\mathbf{m}, \operatorname{div}_{1,\Delta}(h\nabla_{1,\Delta}\mathbf{u}^T))_{T_d} \quad (25)$$

where

$$(\mathbf{a}, \mathbf{b})_{T_d} = \sum_{i,j} \Delta y \Delta x \langle \mathbf{a}_{ij}, \mathbf{b}_{ij} \rangle_{\mathbb{R}^d}.$$

Proof of Lemma 3.2. Thanks to definitions (23)–(24) we have

$$\begin{aligned} (\partial_{x,1\Delta}^0(h\partial_{x,1\Delta}m^x))_{i,j} &= \frac{1}{(\Delta x)^2} (h_{i+1/2,j} (m_{i+1,j}^x - m_{i,j}^x) - h_{i-1/2,j} (m_{i,j}^x - m_{i-1,j}^x)) \\ (\partial_{y,1\Delta}^{00}(h\partial_{x,1\Delta}^{00}m^y))_{i,j} &= \frac{1}{4\Delta y \Delta x} (h_{i,j+1} (m_{i+1,j+1}^y - m_{i-1,j+1}^y) - h_{i,j-1} (m_{i+1,j-1}^y - m_{i-1,j-1}^y)) \\ (\partial_{x,1\Delta}^{00}(h\partial_{y,1\Delta}^{00}m^x))_{i,j} &= \frac{1}{4\Delta y \Delta x} (h_{i+1,j} (m_{i+1,j+1}^x - m_{i+1,j-1}^x) - h_{i-1,j} (m_{i-1,j+1}^x - m_{i-1,j-1}^x)) \\ (\partial_{y,1\Delta}^0(h\partial_{y,1\Delta}m^y))_{i,j} &= \frac{1}{(\Delta y)^2} (h_{i,j+1/2} (m_{i,j+1}^y - m_{i,j}^y) - h_{i,j-1/2} (m_{i,j}^y - m_{i,j-1}^y)) \end{aligned}$$

where we take

$$h_{i+1/2,j} = \frac{1}{2}(h_{i+1,j} + h_{i,j}), \quad h_{i,j+1/2} = \frac{1}{2}(h_{i,j+1} + h_{i,j}).$$

It follows

$$\begin{aligned} (\mathbf{u}, \operatorname{div}(h\nabla\mathbf{m}^T))_{T_d} &= \sum \Delta y \Delta x u_{i,j}^x \frac{1}{(\Delta x)^2} (h_{i+1/2,j} (m_{i+1,j}^x - m_{i,j}^x) - h_{i-1/2,j} (m_{i,j}^x - m_{i-1,j}^x)) \\ &+ \sum \Delta y \Delta x \left(u_{i,j}^x \frac{1}{4\Delta y \Delta x} (h_{i,j+1} (m_{i+1,j+1}^y - m_{i-1,j+1}^y) - h_{i,j-1} (m_{i+1,j-1}^y - m_{i-1,j-1}^y)) \right) \\ &+ \sum \Delta y \Delta x \frac{1}{4\Delta y \Delta x} u_{i,j}^y (h_{i+1,j} (m_{i+1,j+1}^x - m_{i+1,j-1}^x) - h_{i-1,j} (m_{i-1,j+1}^x - m_{i-1,j-1}^x)) \\ &+ \sum \Delta y \Delta x \frac{1}{(\Delta y)^2} u_{i,j}^y (h_{i,j+1/2} (m_{i,j+1}^y - m_{i,j}^y) - h_{i,j-1/2} (m_{i,j}^y - m_{i,j-1}^y)). \end{aligned}$$

We compute successively

$$\begin{aligned} &\sum \frac{\Delta y \Delta x}{(\Delta x)^2} u_{i,j}^x (h_{i+1/2,j} (m_{i+1,j}^x - m_{i,j}^x) - h_{i-1/2,j} (m_{i,j}^x - m_{i-1,j}^x)) \\ &= \sum \frac{\Delta y \Delta x}{(\Delta x)^2} ((u_{i-1,j}^x h_{i-1/2,j} m_{i,j}^x - u_{i,j}^x h_{i+1/2,j} m_{i,j}^x) - (u_{i,j}^x h_{i-1/2,j} m_{i,j}^x - u_{i+1,j}^x h_{i+1/2,j} m_{i,j}^x)) \\ &= \sum \frac{\Delta y \Delta x}{(\Delta x)^2} m_{i,j}^x ((u_{i+1,j}^x - u_{i,j}^x) h_{i+1/2,j} - (u_{i,j}^x - u_{i-1,j}^x) h_{i-1/2,j}) \\ &= \sum \frac{\Delta y \Delta x}{(\Delta x)^2} m_{i,j}^x (h_{i+1/2,j} (\partial_{x,1\Delta} u^x)_{i+1/2,j} - h_{i-1/2,j} (\partial_{x,1\Delta} u^x)_{i-1/2,j}) \\ &= \sum \Delta y \Delta x m_{i,j}^x \partial_{x,1\Delta}^0 (h (\partial_{x,1\Delta} u^x))_{i,j} \end{aligned}$$

and

$$\begin{aligned} &\sum \frac{\Delta y \Delta x}{4\Delta y \Delta x} u_{i,j}^x (h_{i,j+1} (m_{i+1,j+1}^y - m_{i-1,j+1}^y) - h_{i,j-1} (m_{i+1,j-1}^y - m_{i-1,j-1}^y)) \\ &= \sum \frac{\Delta y \Delta x}{4\Delta y \Delta x} (u_{i,j}^x h_{i,j+1} m_{i+1,j+1}^y - u_{i,j}^x h_{i,j+1} m_{i-1,j+1}^y - u_{i,j}^x h_{i,j-1} m_{i+1,j-1}^y + u_{i,j}^x h_{i,j-1} m_{i-1,j-1}^y) \\ &= \sum \frac{\Delta y \Delta x}{4\Delta y \Delta x} m_{i,j}^y (u_{i-1,j-1}^x h_{i-1,j} - u_{i+1,j-1}^x h_{i+1,j} - u_{i-1,j+1}^x h_{i-1,j} + u_{i+1,j+1}^x h_{i+1,j}) \\ &= \sum \frac{\Delta y \Delta x}{4\Delta y \Delta x} m_{i,j}^y ((u_{i+1,j+1}^x - u_{i+1,j-1}^x) h_{i+1,j} - (u_{i-1,j+1}^x - u_{i-1,j-1}^x) h_{i-1,j}) \\ &= \sum \Delta y \Delta x m_{i,j}^y (\partial_{y,1\Delta}^{00} (h \partial_{x,1\Delta}^{00} u^x))_{i,j}. \end{aligned}$$

So that with

$$\begin{aligned} &\sum \frac{\Delta y \Delta x}{4\Delta y \Delta x} u_{i,j}^y (h_{i+1,j} (m_{i+1,j+1}^x - m_{i+1,j-1}^x) - h_{i-1,j} (m_{i-1,j+1}^x - m_{i-1,j-1}^x)) \\ &= \sum \Delta y \Delta x m_{i,j}^x (\partial_{y,1\Delta}^{00} (h \partial_{y,1\Delta}^{00} u^y))_{i,j} \end{aligned}$$

and

$$\begin{aligned} &\sum \Delta y \Delta x \frac{1}{(\Delta y)^2} u_{i,j}^y (h_{i,j+1/2} (m_{i,j+1}^y - m_{i,j}^y) - h_{i,j-1/2} (m_{i,j}^y - m_{i,j-1}^y)) \\ &= \sum \Delta y \Delta x m_{i,j}^y \partial_{y,1\Delta}^0 (h (\partial_{y,1\Delta} u^y))_{i,j}. \end{aligned}$$

We get finally

$$\begin{aligned} (\mathbf{u}, \operatorname{div}_{1,\Delta} (h\nabla_{1,\Delta} \mathbf{m}^T))_{T_d} &= \left(\mathbf{m}, \left(\begin{array}{l} (\partial_{x,1\Delta}^0 (h \partial_{x,1\Delta} u^x)) + (\partial_{y,1\Delta}^{00} (h \partial_{x,1\Delta}^{00} u^y)) \\ (\partial_{x,1\Delta}^{00} (h \partial_{y,1\Delta} u^x)) + (\partial_{y,1\Delta}^0 (h \partial_{y,1\Delta} u^y)) \end{array} \right) \right) \\ &= (\mathbf{m}, \operatorname{div}_{1,\Delta} (h\nabla_{1,\Delta} \mathbf{u}^T))_{T_d}. \end{aligned}$$

Proposition 3.3 *Let us suppose that $\text{div}_{1,\Delta}(h\nabla_{1,\Delta}\mathbf{m}^T)$ satisfies identity (25) of Lemma 3.2, then the capillary step*

$$\mathbf{U}_K^{n+1} = \mathbf{U}_K^{n+1/2} + \Delta t \mathbf{M}_K^{n+1}$$

admits a unique solution which satisfies an energy inequality:

$$\sum_K E_{tot}(\mathbf{U}_K^{n+1}) m_K \leq \sum_K E_{tot}(\mathbf{U}_K^{n+1/2}) m_K. \quad (26)$$

Proof of Proposition 3.3. Let us first prove that the system (18) admits a unique solution. Indeed, one can write $\mathbf{M}_K^{n+1} = \mathcal{M}(h^{n+1}, \mathbf{v}^{n+1/2})(\mathbf{U}_K^{n+1})$ and $\mathcal{M}(h^{n+1}, \mathbf{v}^{n+1/2})$ satisfies

$$(\mathbf{U}, \mathcal{M}(h^{n+1}, \mathbf{v}^{n+1/2})(\mathbf{U}))_{T_d} = 0 \text{ for all } \mathbf{U}$$

from which we deduce that $\mathcal{M}(h^{n+1}, \mathbf{v}^{n+1/2})$ is a skew-symmetric matrix for the scalar product $(\cdot, \cdot)_{T_d}$. Thus its eigenvalues are purely imaginary and $\text{Id} - \Delta t \mathcal{M}(h^{n+1}, \mathbf{v}^{n+1/2})$ is invertible. Now, thanks to identity (18) and the convexity of E_{tot} (the fluid height h is assumed $h > 0$):

$$E_{tot}(\mathbf{U}_K^{n+1}) \leq E_{tot}(\mathbf{U}_K^{n+1/2}) - \Delta t \nabla_{\mathbf{U}} E_{tot}(\mathbf{U}_K^{n+1})^T \mathbf{M}_K^{n+1}.$$

Denote $f^{n+1/2} = f(h_K^{n+1}, \mathbf{v}_K^{n+1/2})$, $\mathbf{g}^{n+1/2} = \mathbf{g}(h_K^{n+1}, \mathbf{v}_K^{n+1/2})$ and $DE := \sum_K \nabla_{\mathbf{U}} E_{tot}(\mathbf{U}_K^{n+1})^T \mathbf{M}_K^{n+1} m_K$.

$$R = - \left(\mathbf{u}_K^{n+1}, \nabla_{3,\Delta} \left(g^{n+1/2} \mathbf{v}_K^{n+1} \right) \right)_{T_d} - \left(g^{n+1/2} \mathbf{v}_K^{n+1}, \text{div}_{3,\Delta}(\mathbf{u}_K^{n+1}) \right)_{T_d}$$

and

$$D = \left(\mathbf{u}_K^{n+1}, \text{div}_{1,\Delta} \left(h_K^{n+1} \nabla_{1,\Delta} \left(f^{n+1/2} \mathbf{v}_K^{n+1} \right)^T \right) \right)_{T_d} - \left(\text{div}_{1,\Delta} \left(h_K^{n+1} \nabla_{1,\Delta}(\mathbf{u}_K^{n+1})^T \right), f^{n+1/2} \mathbf{v}_K^{n+1} \right)_{T_d}$$

We easily get that $DE = R + D$. As a consequence of definition 20, we get directly $R = 0$, and, as a consequence of lemma 3.2, we get $D = 0$. It follows that

$$\sum_K E_{tot}(\mathbf{U}_K^{n+1}) m_K \leq \sum_K E_{tot}(\mathbf{U}_K^{n+1/2}) m_K.$$

We thus have proved the following stability result.

Proposition 3.4 *Consider the scheme (15)–(18)–(19) with discretization (24) of capillary terms, then provided a CFL condition of the type (17) is satisfied, the fluid height h is positive and the scheme satisfies energy stability*

$$\sum_K E_{tot}(\mathbf{U}_K^{n+1}) m_K \leq \sum_K E_{tot}(\mathbf{U}_K^n) m_K.$$

This stability result can be extended to a more general numerical framework and other time discretizations. By taking discrete dual operators with similar rules as (20) namely

$$(\mathbf{w}, \text{div}_{1,\Delta}(\mathcal{T}))_T = -(\nabla_{1,\Delta} \mathbf{w}, \mathcal{T})_{T_d}$$

We thus get

$$\begin{aligned} D &= \left(\mathbf{u}_K^{n+1}, \text{div}_{1,\Delta} \left(h_K^{n+1} \nabla_{1,\Delta} \left(f^{n+1/2} \mathbf{v}_K^{n+1} \right)^T \right) \right)_{T_d} - \left(\text{div}_{1,\Delta} \left(h_K^{n+1} \nabla_{1,\Delta}(\mathbf{u}_K^{n+1})^T \right), f^{n+1/2} \mathbf{v}_K^{n+1} \right)_{T_d} \\ &= - \left(\nabla_{1,\Delta} \mathbf{u}_K^{n+1}, h_K^{n+1} \nabla_{1,\Delta} \left(f^{n+1/2} \mathbf{v}_K^{n+1} \right)^T \right)_{T_d} - \left(\text{div}_{1,\Delta} \left(h_K^{n+1} \nabla_{1,\Delta}(\mathbf{u}_K^{n+1})^T \right), f^{n+1/2} \mathbf{v}_K^{n+1} \right)_{T_d} \\ &= - \left(\nabla_{1,\Delta} \left(f^{n+1/2} \mathbf{v}_K^{n+1} \right), h_K^{n+1} \nabla_{1,\Delta}(\mathbf{u}_K^{n+1})^T \right)_{T_d} - \left(\text{div}_{1,\Delta} \left(h^{n+1} \nabla_{1,\Delta}^t \mathbf{u}_K^{n+1} \right), f^{n+1/2} \mathbf{v}_K^{n+1} \right)_{T_d} \\ &= \left(f^{n+1/2} \mathbf{v}_K^{n+1}, \text{div}_{1,\Delta} \left(h_K^{n+1} \nabla_{1,\Delta}(\mathbf{u}_K^{n+1})^T \right) \right)_{T_d} - \left(\text{div}_{1,\Delta} \left(h_K^{n+1} \nabla_{1,\Delta}(\mathbf{u}_K^{n+1})^T \right), f^{n+1/2} \mathbf{v}_K^{n+1} \right)_{T_d} \\ &= 0 \end{aligned}$$

Condition (25) of Lemma 3.2 is valid and also insures energy stability result of Proposition 3.3.

One could also consider alternative time discretization like the fully implicit scheme for the capillary step:

$$\mathbf{U}^{n+1} = \mathbf{U}^{n+1/2} + \Delta t \mathcal{M}(h^{n+1}, \mathbf{U}^{n+1})(\mathbf{U}^{n+1}) \quad (27)$$

This system could be solved through an iterative scheme:

$$\mathbf{U}^{n+1,p+1} = \mathbf{U}^{n+1/2} + \Delta t \mathcal{M}(h^{n+1}, \mathbf{U}^{n+1,p})(\mathbf{U}^{n+1,p+1}), \quad \mathbf{U}^{n+1,0} = \mathbf{U}^{n+1/2}. \quad (28)$$

The linear system (28) admits a unique solution which, moreover, satisfies the energy estimate

$$\sum_K E_{tot}(\mathbf{U}_K^{n+1,p}) m_K \leq \sum_K E_{tot}(\mathbf{U}_K^{n+1/2}) m_K, \quad \forall p \geq 0.$$

If Δt is small enough so that $\|\delta t \mathcal{M}(h_K^{n+1}, \mathbf{v}_K^{n+1/2})\| < 1$, the sequence $(\mathbf{U}_K^{n+1,p})_{p \in \mathbb{N}}$ converges to \mathbf{U}_K^{n+1} which, in turn, satisfies

$$\sum_K E_{tot}(\mathbf{U}_K^{n+1}) m_K \leq \sum_K E_{tot}(\mathbf{U}_K^{n+1/2}) m_K \leq \sum_K E_{tot}(\mathbf{U}_K^n) m_K.$$

As a result, the IMPLICIT-EXPLICIT scheme build on a time discretization with explicit steps for the hyperbolic part and implicit steps for the capillary part are entropy stable. This provides a method to design higher order in time IMPLICIT-EXPLICIT schemes which are build on fully implicit time discretizations.

4 Numerical Simulations

We present in this section various numerical simulations to illustrate the benefits of the proposed extended model. The new extended system composed by a conservative hyperbolic part and a second order derivative part which is skew symmetric for the L^2 scalar product is crucial to develop an appropriate splitting method.

We are able to carry out extremely fast simulations of capillary wave propagation in comparison to direct numerical simulations of the original Navier-Stokes equations (DNS). On the one hand, this is due to the vertical integration along the fluid height which reduces the dimension of the problem and withdraw the initial free surface problem. On the other hand, the implicit treatment of surface tension removes the classical restrictive capillary time step, empirically based to the fastest “eligible” wave speed whose wavelength is the grid size. We will illustrate both the overall stability of the numerical method and the interest of considering the full surface tension source term.

Global energy dissipation will be shown on time discretizations that are first order accurate. The time discretization is of IMPLICIT-EXPLICIT type: for the hyperbolic part, an explicit Euler time-stepping scheme has been used, associated with a Rusanov flux,

$$G_{e,K}^n = G(\mathbf{U}_{e,K}^n, \mathbf{U}_{e,K_e}^n, \mathbf{n}_{e,K}) = \frac{F(\mathbf{U}_{e,K}^n) + F(\mathbf{U}_{e,K_e}^n)}{2} - \max_{K,K_e} \left(|\mathbf{u} \cdot \mathbf{n}_{e,K}| + \sqrt{g_r h} \right) \frac{\mathbf{U}_{e,K_e}^n - \mathbf{U}_{e,K}^n}{2},$$

using the rotational invariance and considering second-order in space MUSCL reconstructions denoted by $\mathbf{U}_{e,K}^n$ and \mathbf{U}_{e,K_e}^n of the primitive variables (without limitation as very smooth solution will be considered here) whereas an implicit Euler time-stepping scheme is used for the capillary step, by considering a simpler linearized resolution of the initial fully nonlinear problem of coupled equations. While other reconstruction method are possible and can lead to higher order accuracy, the MUSCL method is a second order method that is easy to implement and has the advantage to be suitable with structured and unstructured mesh. The model has been coded on an unstructured environment, and it is planned to run simulations with it once we have solved the discrete duality problem in such context.

It should be noted that a global second-order solver can be derived by considering an appropriate IMEX time-stepping scheme to combine the explicit and implicit steps but this strategy is costly as it requires to solve the full nonlinear problem, that can be achieved using Newton-like method or simply iterating on the linearized version of the initial full nonlinear problem of coupled equations until convergence.

4.1 Numerical Set Up

We consider a rectangular domain $[0, l_x] \times [0, l_y]$ divided into $n_x \times n_y$ cells considering uniform discretization steps Δx and Δy respectively in each direction. In a Finite Volume framework, the $h_{i,j}$ and $\mathbf{u}_{i,j}$ discrete unknowns are associated classically to the mean of respectively a scalar field h and a vector field \mathbf{u} over the appropriate cell. In order to avoid any specific treatment of boundary conditions, we have only considered *periodic boundary conditions*.

We have carried out numerical simulations of the augmented version of the shallow water equations in two situations: the quadratic capillary case and the fully nonlinear capillary case. In the quadratic case, the system (9,10) is written with,

$$E(h, \nabla h) = g_r \frac{h}{2} + \frac{1}{2} \frac{\sigma}{\rho} \|\nabla h\|^2, \quad (29)$$

meaning,

$$\mathcal{E}_{\text{cap}}(q) = \frac{1}{2} q^2, \quad \kappa(h) = \frac{\sigma}{\rho}, \quad \alpha(q^2) = 1,$$

and

$$f(h, \mathbf{v}) = \sqrt{h} \sqrt{\frac{\sigma}{\rho}} \text{Id}, \quad \mathbf{g}(h, \mathbf{v}) = \frac{h\mathbf{v}}{2},$$

where g_r , σ and ρ are respectively the constant gravity acceleration, the surface tension coefficient and the constant density of the flow. In the fully nonlinear capillary case, the system (9,10) is defined with,

$$E(h, \nabla h) = g_r \frac{h}{2} + \frac{\sigma}{\rho} (\sqrt{1 + \|\nabla h\|^2} - 1), \quad (30)$$

meaning,

$$\mathcal{E}_{\text{cap}}(q) = \sqrt{1 + q^2} - 1, \quad \kappa(h) = \frac{\sigma}{\rho}, \quad \alpha(q^2) = \sqrt{2} \left(1 + \sqrt{1 + q^2}\right)^{-1/2},$$

and

$$f(h, \mathbf{v}) = \sqrt{h} \left(1 + \frac{\rho h}{4\sigma} \|\mathbf{v}\|^2\right)^{-1/2} \left(\text{Id} - \left(1 + \frac{\rho h}{2\sigma} \|\mathbf{v}\|^2\right)^{-1} \frac{\rho h}{4\sigma} \mathbf{v} \otimes \mathbf{v}\right), \quad \mathbf{g}(h, \mathbf{v}) = \frac{h\mathbf{v}}{2} \left(1 + \frac{\rho h}{2\sigma} \|\mathbf{v}\|^2\right)^{-1}.$$

We recall that the expression of \mathbf{v} as a function of α and κ is given in Equation (8).

4.2 One-dimensional simulation with Gaussian initial data

We consider a one-dimensional Gaussian-shaped deformation of the free surface of a water layer, as illustrated in Figure (2). This deformation produces both gravity and capillary waves whose relative influence is measured by the Eötvös number, also called Bond number,

$$\text{Eo} = \text{Bo} = \frac{\rho g_r h^2}{\sigma}, \quad (31)$$

as long as the shape of the Gaussian is close to the shape of a drop, i.e. its curve peak height is comparable to its width. We set physical parameters to the conventional values for water at room temperature and are summarized in Table (1).

$$\begin{aligned} \sigma &= 0.0728 \text{ N m}^{-1} \\ \rho &= 1000 \text{ kg m}^{-3} \\ \nu &= 10^{-6} \text{ m}^2 \text{ s}^{-1} \\ g_r &= 9.81 \text{ m s}^{-2} \end{aligned}$$

Table 1: Physical parameters for the simulations.

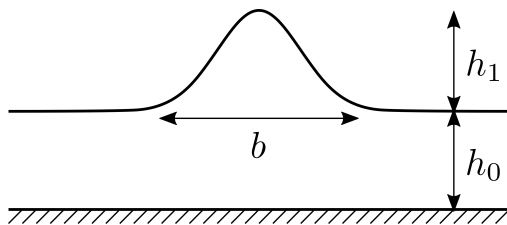


Figure 2: One-dimensional sketch of the Gaussian deformation of a layer of water where b is the full width at tenth of maximum (FWTM).

The initial Gaussian-shaped deformation of the water layer parametrizes the initial surface elevation as,

$$h(x, t = 0) = h_0 + h_1 e^{-\frac{x^2}{2(b/b_0)^2}}, \quad (32)$$

with $b_0 = 4.29193$ allowing to consider approximately the full width at tenth of maximum as the length b represented in the Figure (2). As the Eötvös number Eq.(31) is set to 1, such that gravity and capillary waves are generated in the same time order, this gives a water deformation peak elevation $h_1 = 2.725$ mm. The layer of water elevation at rest is set to $h_0 = h_1$ whereas the full width at tenth of maximum is set to $b = 1.5 h_1$. The computational domain is set to $[-50\text{mm}, 50\text{mm}]$ and the simulation time to 5 ms in order to produce significant waves in order to compare the results with the two models with respectively a linearized capillary contribution and a full nonlinear capillary contribution. Finally, the initial velocity is set to zero and the auxiliary variable v is initialized through the formulas according to the two models considered. In practice, it is not needed to compute exactly ∇h , a simple discretization using a classic centered scheme for example is sufficient and used here in practice.

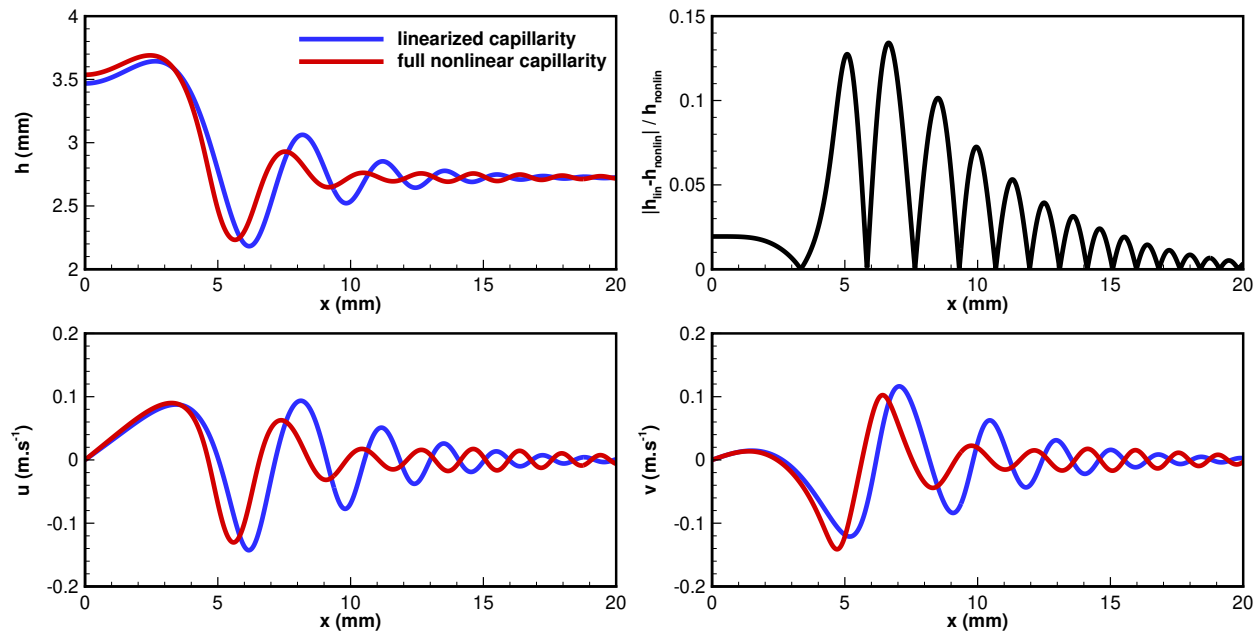


Figure 3: Very fine (51200 cells) resolved numerical simulations of capillary-gravity waves considering a one-dimensional Gaussian-shaped deformation of a layer of water using the proposed augmented shallow-water model Eq.(9,10) and formulas Eq.(29,30). Only a window of the real computational domain is plotted since the simulations are symmetric around zero and the waves not significant far away from zero; (top-left) Water height h ; (top-right) Relative difference between the two water heights; (bottom-left) Velocity u ; (bottom-right) Auxiliary velocity v .

It is presented in Figure (3) the very fine resolved results for the water height h , the velocity \mathbf{u} and the auxiliary velocity \mathbf{v} considering the two proposed models. For the physical parameters and space scaling chosen, there is a significant difference between the two models since the gradient of the water height ∇h is sufficiently large to observe such a behaviour. The computation of the relative difference between the water height of each model shows an approximate maximal difference of 14%. This is not only due to the difference in the capillary wave amplitude, but also to an important phase shift.

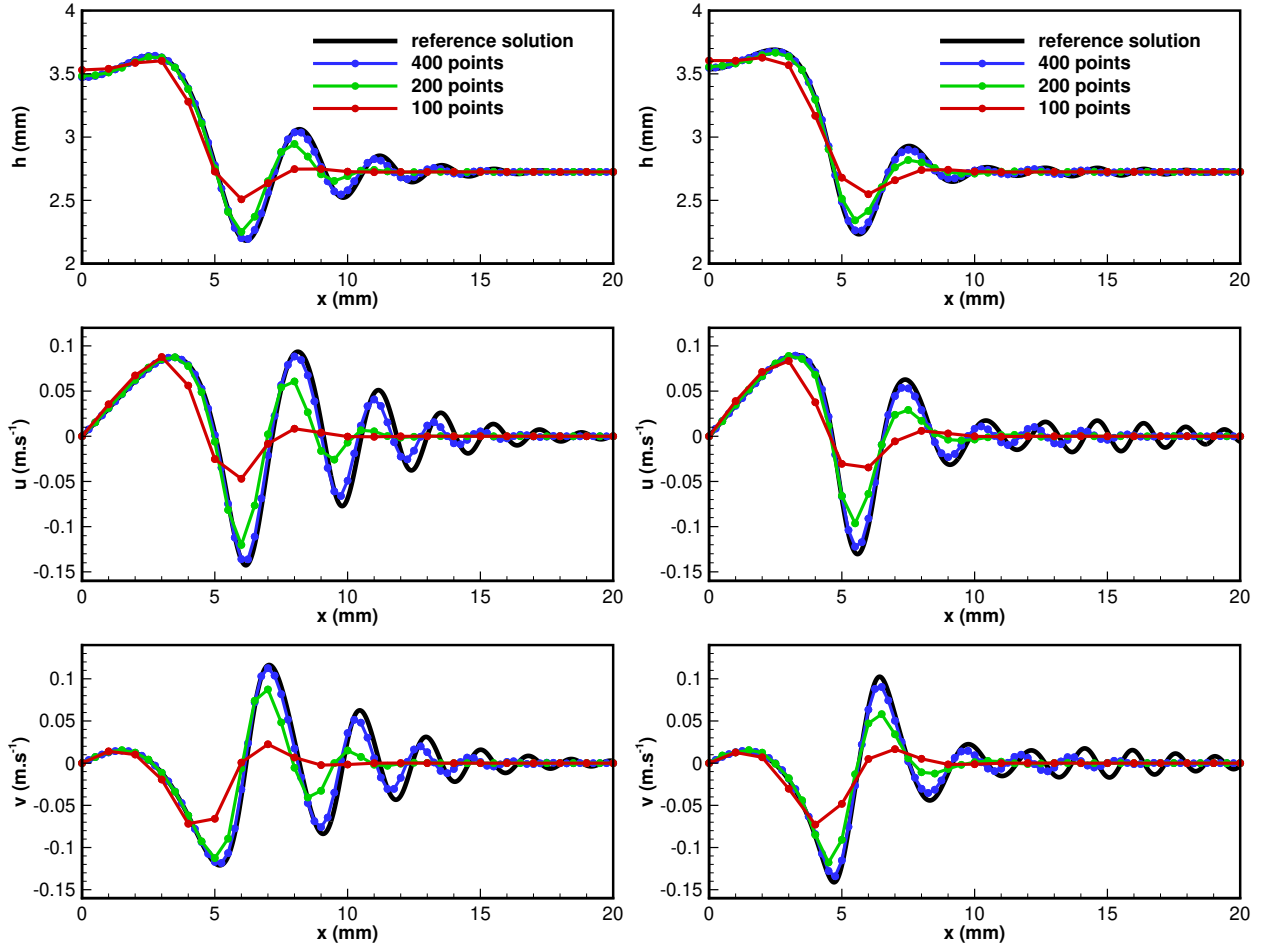


Figure 4: Same simulations than for Figure (3), but for the first grid sizes considered in order to materialize the numerical solution quality with a growing number of discretization points in the characteristic wavelength; (left) with the linearized capillary contribution; (right) with the full nonlinear capillary contribution.

The computational simulation time being 5 ms, it can also be observed that the capillary waves phase velocity are much larger than the fluid velocity. This can be easily explained by studying the dispersion relation, developed around a layer with a height h_0 and a zero velocity, giving a wave speed,

$$c \approx u \pm \sqrt{g_r h_0 + \frac{h_0 \sigma}{\rho} k^2}. \quad (33)$$

where k denotes the wave number of a plane wave. The ratio between the capillary wave speed and gravity wave speed is then approximately equal to $\sqrt{\sigma/g_r \rho} 2\pi/\lambda \approx 0.017/\lambda$, where λ is the characteristic wavelength of the surface elevation. As the Fourier transform of an initial Gaussian-shape deformation is again a Gaussian, there are wavelengths as small as the machine accuracy allows to capture. Thus, for plane waves with a wavelength of 0.17 mm, the capillary wave speed is 100 times faster than the gravity wave speed. This is the reason why we have chosen a CFL number based on the maximal absolute eigenvalue

of the hyperbolic Jacobian matrix at an arbitrary value of 0.01 in order to capture the propagation of the capillary waves. Whereas proposed numerical discretization allows to work with higher CFL numbers close to 1 due to the implicit resolution of the source terms modelling the full contribution of the surface tension, the induced larger time steps imply a numerical time capturing low pass filter regarding the capillary waves. Another numerical viewpoint of using CFL numbers close to 1 is that the induced linear system resolution becomes more difficult due to a growing condition number of the resulted matrix with larger time steps. In other words, the numerical resolution is computationally more expensive whereas less physical phenomenon of the capillary action is captured.

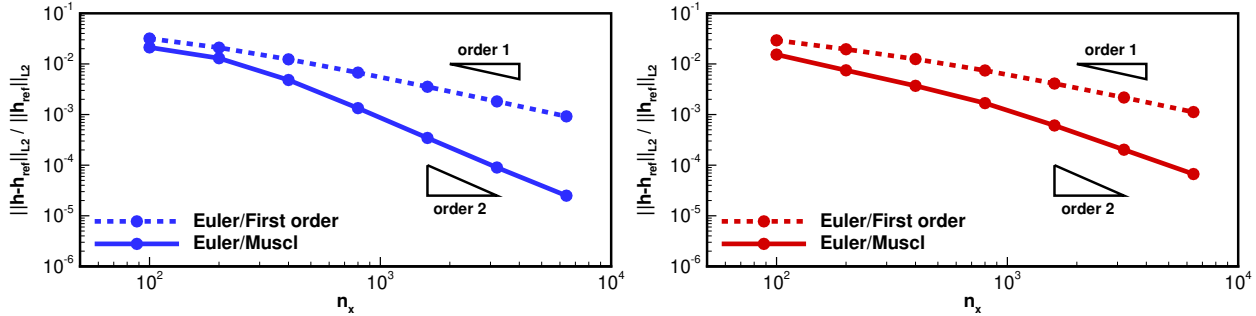


Figure 5: Relative error for the water height h in the L_2 norm as a function of the grid size, computed at the end of the simulation given a reference solution h_{ref} computed with 51200 points; (left) with the linearized capillary contribution; (right) with the full nonlinear capillary contribution.

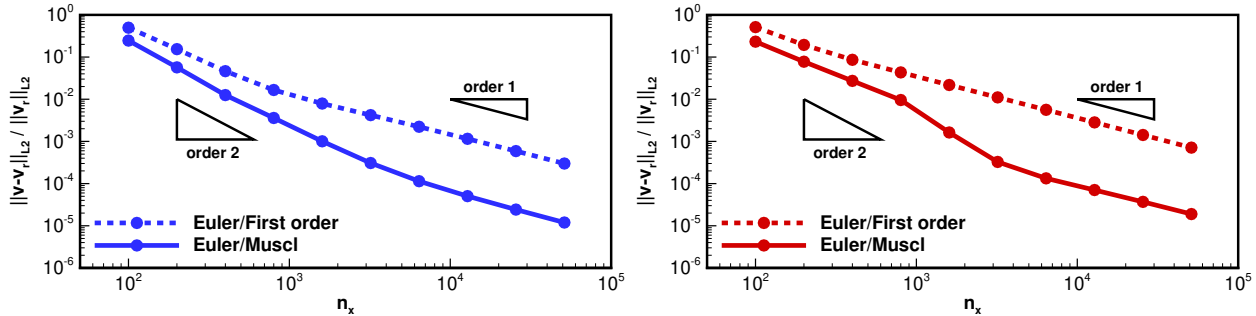


Figure 6: Relative error for the auxiliary velocity v in the L_2 norm as a function of the grid size, comparatively to the velocity v_r recomputed from h and its gradient ∇h for the same grid size; (left) with the linearized capillary contribution; (right) with the full nonlinear capillary contribution.

A convergence study has been made for these same parameters, considering different grid resolution in space, with a CFL number fixed to 0.01. The complete results for the water elevation h , the fluid velocity u and the auxiliary velocity v and for the first grid sizes of 100, 200 et 400 points for are given in Figure (4), for the linearized capillary contribution version of the model as well as the full capillary contribution version, in order to materialize the numerical solution quality. The relative error for the water height h in the L_2 norm has been plotted in Figure (5), computed at the end of the simulation given a previous reference solution computed with 51200 points. This has been made with both first and second order schemes in space (without and with MUSCL reconstructions, with no limitation as the solution is very smooth). The benefit of the MUSCL reconstruction can be clearly noticed, especially as soon as the meshes are of medium size, when the characteristic wavelength is meshed by more than approximately 10 points. However, an asymptotic convergence of 1 should be found increasing mesh grid sizes due to the use of a first order time-stepping scheme. But the finest mesh used of 6400 points is not yet fine enough to find it. It is validating partially the choice to use a simple split explicit/implicit Euler time-stepping scheme rather than a more sophisticated IMEX time-stepping method. Indeed, an IMEX time-stepping scheme at second order requires more than ten times of computational time in the present case, due to the mandatory resolution of the full nonlinear

problem, knowing that the consistency error in space is predominant over the error in time.

The relative error for the auxiliary velocity \mathbf{v} in the L_2 norm as a function of the grid size has been plotted in Figure (6), comparatively to the velocity \mathbf{v}_r , recomputed from h and its gradient ∇h for the same grid size. The purpose is to check if the velocity field \mathbf{v} once advected in time is still the one that carries the capillary energy as defined by the Eq.(8). And we can verify that this is the case as it naturally converges with the grid size as the numerical consistency errors and the residual error in the linear system resolution deviate \mathbf{v} from the “right” solution. But even for very coarse meshes, the relative error is relatively low and of course even more with MUSCL reconstructions. Also note that the relative error is slightly more important when the full nonlinear capillary contribution version is used.

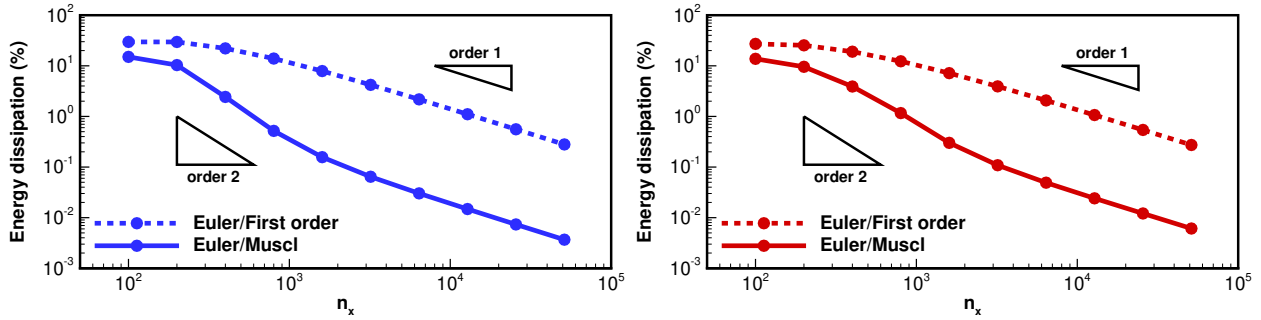


Figure 7: Amount of energy dissipation in percents as a function of the grid size, computed at the end of the simulation following the formula $E = gh^2/2 + h \|\mathbf{u}\|^2/2 + h \|\mathbf{v}\|^2/2$; (left) with the linearized capillary contribution; (right) with the full nonlinear capillary contribution.

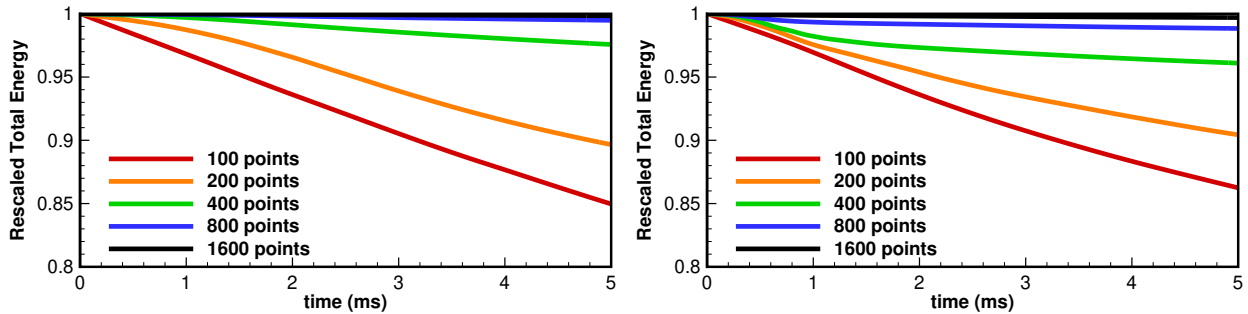


Figure 8: Evolution in time of the energy for the first grid sizes considered; (left) with the linearized capillary contribution; (right) with the full nonlinear capillary contribution.

The amount of energy dissipation in percents as a function of the grid size is shown in Figure (7). We recall that the energy is strictly dissipated at each time step as it has been demonstrated previously. It can be verified that this is indeed the case in practice by looking at Figure (8). The energy can be interpreted as an L_2 norm with the advantage to check in one measure all the contributions in the numerical system, rather than to check separately the convergence in a chosen norm for the water height h and the two velocities \mathbf{u} and \mathbf{v} . For very coarse meshes, representing few points in the characteristic wavelength, see Figure (4), approximately 10% of energy dissipation is found, which is relatively acceptable with regard to the grid resolution used. Using MUSCL reconstruction for finer meshes, an extra rate of convergence greater than 2 is reached before falling to the theoretical asymptotic rate of 1 for very fine meshes. Whereas, without MUSCL reconstructions, the convergence rate begin at a value lower than 1, giving quickly significant differences, before reaching asymptotically the same theoretical convergence rate of 1 for very fine meshes. It gives finally an important order of magnitude difference of approximately 2 when the characteristic wavelength is sufficiently meshed with more than 10 points.

4.3 Two-dimensional simulations with Gaussian initial data

A two-dimensional version of the same previous problem (4.2) is now considered. The initial Gaussian-shaped deformation of a layer of water is materialised initialising the water elevation by,

$$h(x, y, t = 0) = h_0 + h_1 e^{-\frac{x^2 + y^2}{2(b/b_0)^2}} \quad (34)$$

The physical parameters are the same than ones summarised in the Tab.(1), as well as the space scaling with an Etvös number again chosen to 1, giving a layer of water deformation elevation $h_1 = h_0 = 2.725$ mm, and a full width at tenth of maximum again fixed to $b = 1.5 h_1$. The computational domain is set to $[-50 \text{ mm}, 50 \text{ mm}]^2$ and the simulation time to 5 ms.

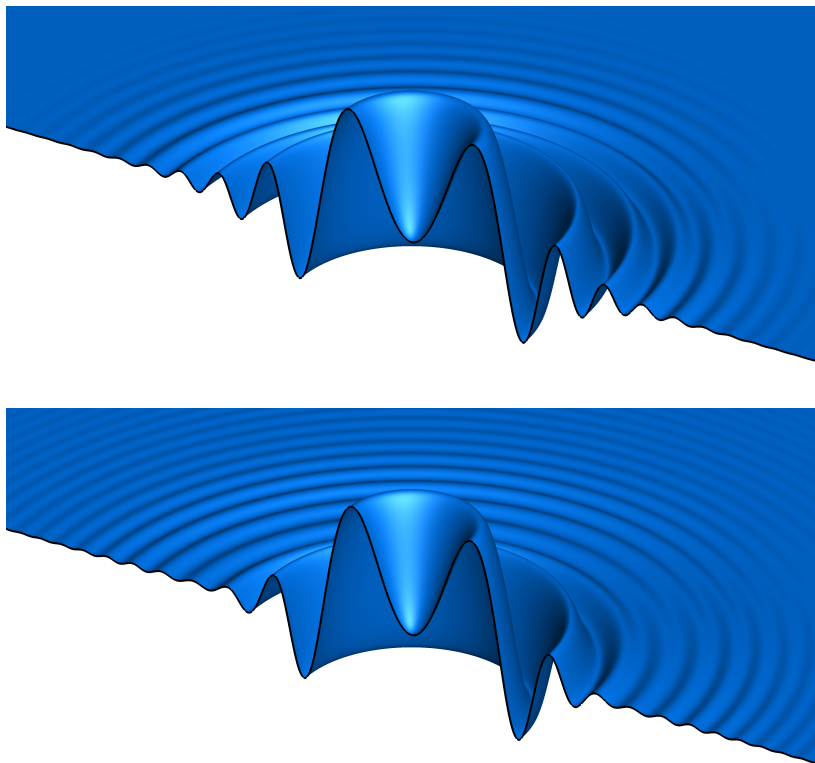


Figure 9: Numerical simulations of capillary-gravity waves considering a two-dimensional Gaussian-shaped deformation of a layer of water, using the proposed augmented model with parameters Eq.(29),(30)) and a 1600×1600 cells grid; (up) with the linearized capillary contribution; (down) with the full nonlinear capillary contribution.

It can be observed in Figure (9) the axisymmetric propagation of capillary-gravity waves using the proposed augmented shallow-water model Eq.(9,10) with formulas Eq.(29,30). The initial peak collapse on his own weight and generate a train of capillary waves. The difference between the two models for the water height h is plotted in Figure (10). It can be observed a maximum difference of 3%. If the same phenomena as in the one-dimensional case can be observed, the initial chosen shape of the Gaussian deformation of the water layer gives lower differences since axisymmetry reduces the capillary waves speed difference and the phase shift generated.

The two-dimensional version behaves like the one-dimensional one, as it can be seen in Figure (11) and in Figure (12). In the same way, the relative error for the auxiliary velocity magnitude $\|\mathbf{v}\|$ comparatively to the recomputed one $\|\mathbf{v}_r\|$ converges with the grid size, and is relatively low even for coarse meshes, with a lower error using MUSCL reconstructions. In addition, it is also shown in Figure (10) a map of the absolute difference showing no particular region with a big peak. The amounts of energy dissipation are only

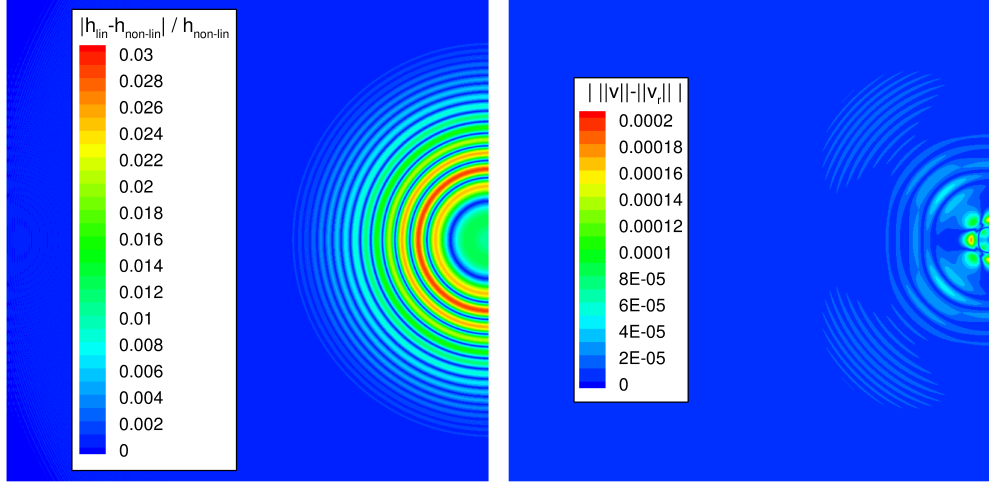


Figure 10: Same simulation than for the Figure (9) with half of the domain in each direction; (left) relative difference between the water height for the two models; (right) absolute difference between the auxiliary velocity magnitude $\|\mathbf{v}\|$ and the velocity magnitude $\|\mathbf{v}_\tau\|$ recomputed from h and its gradient ∇h for the same grid size.

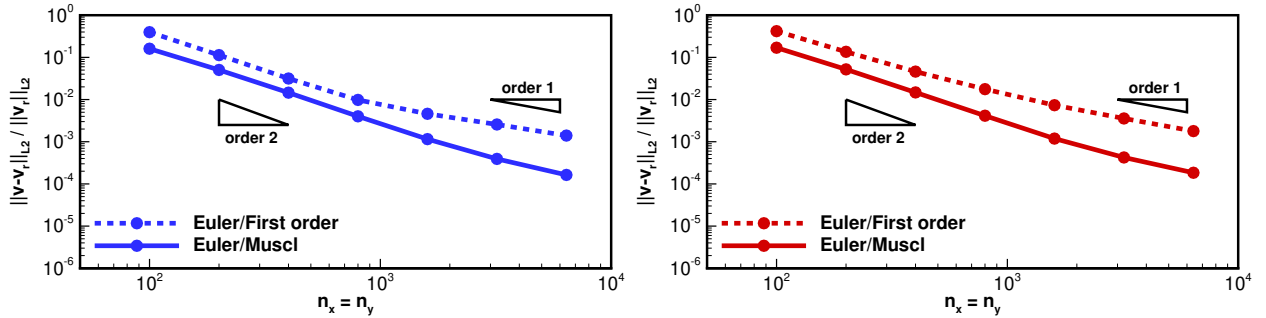


Figure 11: Relative error for the auxiliary velocity magnitude $\|\mathbf{v}\|$ in the L_2 norm as a function of the grid size, comparatively to the same velocity magnitude $\|\mathbf{v}_\tau\|$ recomputed from h and its gradient ∇h for the same grid size; (left) with the linearized capillary contribution; (right) with the full nonlinear capillary contribution.

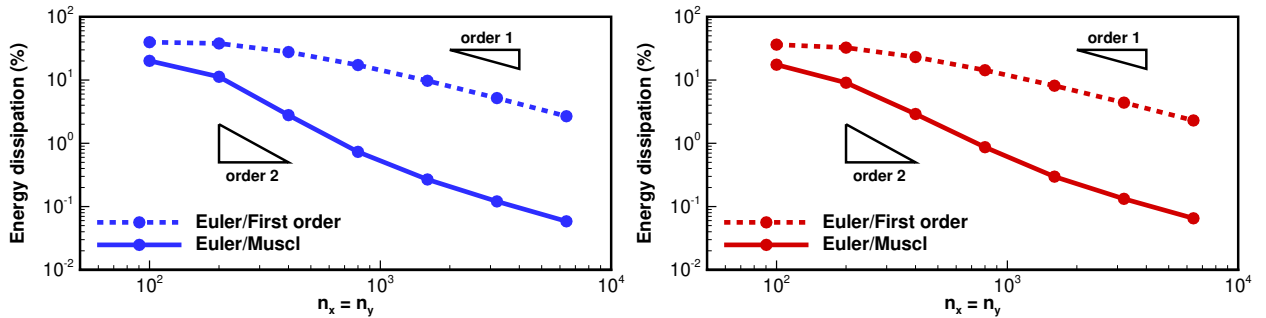


Figure 12: Amount of energy dissipation in percents as a function of the grid size, computed at the end of the simulation following the formula $E = gh^2/2 + h\|\mathbf{u}\|^2/2 + h\|\mathbf{v}\|^2/2$; (left) with the linearized capillary contribution; (right) with the full nonlinear capillary contribution.

slightly higher than for the one-dimensional case. Again, the MUSCL reconstructions provide an extra rate

of convergence near 2 for medium grid sizes before falling asymptotically to the theoretical rate of 1, which finally gives approximately two orders of magnitude of difference if not using it.

This validate the application of the proposed augmented shallow water model Eq.(9,10) for both one- and two-dimensional cases, with very similar numerical convergence behaviour.

4.4 Liquid film falling on a vertical wall

The purpose is now to apply our extended shallow water model with surface tension to a more realistic case of simulation of a liquid film falling on a vertical wall. We are able to compare the resulting numerical solutions with the solutions computed from the `Auto07p` software ([9]). The model used is the one developed by G. Richard and al. [27] written here in non-dimensional form,

$$\begin{aligned} \partial_t h + \partial_x (hu) &= 0 \\ \partial_t (hu) + \partial_x \left(hu^2 + \frac{2}{225} \lambda^2 h^5 + \frac{h^2 \cos \theta}{2\text{Fr}^2} \right) &= \frac{1}{\text{Re}} \left(\lambda h - \frac{3u}{h} \right) + \frac{9}{2\text{Re}} \partial_x (h \partial_x u) + \frac{1}{\text{We}} h \partial_x \mathcal{K} \end{aligned} \quad (35)$$

where \mathcal{K} is the curvature, and its expression is $\partial_{xx}h$ in the linearized case and $\partial_x (\partial_x h / \sqrt{1 + \partial_x h^2})$ in the full nonlinear case. Scales are the film thickness h_N and the Nusselt speed $u_N = gh_N^2 \sin \theta / (3\nu)$. Dimensionless numbers are the Reynolds number $\text{Re} = h_N u_N / \nu = gh_N^3 \sin \theta / (3\nu^2)$, the Froude number $\text{Fr} = u_N / \sqrt{gh_N}$, the Weber number $\text{We} = \rho h_N u_N^2 / \sigma$ and $\lambda = \text{Re} \sin \theta / \text{Fr}^2 = 3$. The Kapitza dimensionless number $\text{Ka} = (\sigma / \rho) (g \sin \theta)^{-1/3} \nu^{-4/3}$ can be added such that $\text{Ka} = \text{Re}^{4/3} \text{Fr}^{2/3} \text{We}^{-1}$.

We have constructed solitary wave solutions to (35) using the `Auto07p` software with the constraint of a constant averaged thickness $\langle h \rangle = 1$. The system of partial differential equations simplifies into ordinary differential equations in the moving frame of reference $\xi = x - ct$, where c refers to the phase speed of the waves. Travelling wave solutions to (35) correspond to limit cycles of the resulting autonomous dynamical system in a phase space of dimension three spanned by the thickness h and its first and second derivatives. Limit cycles are found by continuation starting from a Hopf bifurcation of a fixed point corresponding to the uniform-film solution $h = 1$. Solitary waves are next obtained by increasing the period of the limit cycles. The parameters retained are a vertical wall $\theta = \pi/2$, a Reynolds number $\text{Re} = 80$, a Kapitza number $\text{Ka} = 1000$ and a length $L = 400 h_N$. The liquid corresponds to $\nu = 0.9310 \cdot 10^{-6} \text{ m}^2 \cdot \text{s}^{-1}$, $\rho = 994.3 \text{ kg}$ and $\sigma = 0.019322 \text{ N} \cdot \text{m}^{-1}$ and the gravitational acceleration to $g = 9.81 \text{ m} \cdot \text{s}^{-2}$. The Nusselt film thickness is $h_N = 0.27659 \text{ mm}$ so that the length of the numerical domain is $L = 110.636 \text{ mm}$. The grid comprises 8000 mesh points with spatial adaptation. The spatial discretization uses the method of orthogonal collocation using piecewise polynomials with four collocation points per mesh intervals (2000 mesh intervals). The collocation points are placed to equidistribute the local discretization error in the three-dimensional phase space, which ensures refinement of the mesh at locations of steep gradients. `Auto07p` uses a predictor-corrector algorithm based on a Keller's pseudo-arc length continuation method that enables to detect bifurcations and folds. Details of the algorithm can be found online at <http://indy.cs.concordia.ca/auto/>. Convergence was checked by varying the error tolerances and the number of mesh cells.

Numerical simulations have been carried out using the extended shallow water model system (9,10) defined in exactly the same way as in (29,30). The only differences are a different pressure term in the hyperbolic system changing the Rusanov flux and the introduction of additional source terms treated implicitly simply introducing them in the original linear system arising from the surface tension treatment. A periodic boundary condition and an initial sinusoidal deformation of the film liquid at rest, taking care to a constant mass flow rate, are prescribed. As we are only interested in whether the model is capable of reproducing the solutions given by the `Auto07p` software, only simulations with a very fine mesh size of 25600 cells are presented here. We can observe an almost perfect agreement between the solutions validating the good behaviour of the proposed extended model regarding a produced exact solution from the resolution of ordinary differential equations. It is not presented here but the liquid film deformations are perfectly stable in time.

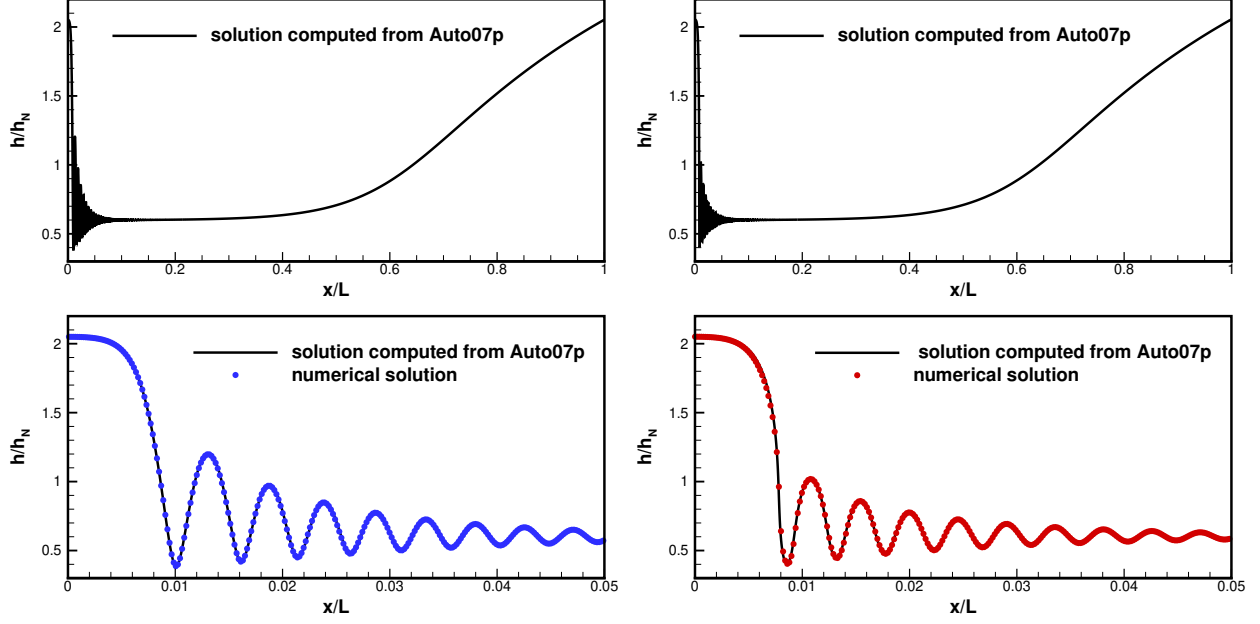


Figure 13: Liquid film falling on a vertical wall at $Re = 80$ and $Ka = 1000$; (top) Complete solutions computed with the `Auto07p` software; (bottom) Comparison between the numerical solutions (one point per ten considering 25600 cells) and the solution computed with the `Auto07p` software with a focus on the capillary ripples; (left) with linearized curvature \mathcal{K} in (35); (right) with full nonlinear curvature \mathcal{K} in (35).

5 Conclusion and Perspectives

In this paper, we have introduced a new extended version of the shallow water equations with surface tension which may be decomposed in two parts: a conservative hyperbolic part and a second order derivative part which is skew-symmetric with respect to the L^2 scalar product. This extended form is suitable for an appropriate splitting method which allows for large gradients of fluid height. The formulation is valid for any non linear form of the capillary energy as a functional of $\|\nabla h\|$. In the case of deep gradient of the free surface the new formulation make possible to deal with complete nonlinear capillary models.

The formulation allows to deal with the capillary terms as a semi-linear skew symmetric problem, and thus associate a semi implicit resolution of the capillary terms, relaxing the time step restriction $\Delta t < Ch^2$ in the original formulation [24] and [3] which are restricted to quadratic forms of the capillary energy. We expect that this property (semi linear implicit treatment of capillary terms) will ensure some robustness and will be successful in the extension of this methodology to wetting problems as in the work of J. Lallement, P. Trontin, C. Laurent and P. Villedieu published in [22] where ad hoc extension with some disjunction pressure are proposed. We recently developed various 3 or 4 equations models (see [28]), for thin film models which are extension of the Korteweg system introduced here. We expect that our formalism also apply to such systems. Nevertheless the question of non-linear stability remains to study. In such case the natural extension of our proofs relies on entropy estimate (related to the so called enstrophy introduced in [28]).

Finally it will be interesting to study possible applications to the solution of Benney type equations obtained as relaxed system of the Shallow water system with friction source terms such as those studied in [27]. This reads, starting from a simplified 2D version,

$$\begin{cases} \partial_t h + \operatorname{div}(h\mathbf{u}) = 0 & (i) \\ \partial_t(h\mathbf{u}) + \operatorname{div}(h\mathbf{u} \otimes \mathbf{u}) + \nabla P = \frac{1}{\varepsilon Re} \left(\lambda h - \frac{3\mathbf{u}}{h} \right) - \operatorname{div}(\nabla h \otimes \nabla_{\mathbf{p}} E) + \nabla(h \operatorname{div}(\nabla_{\mathbf{p}} E)) & (ii) \end{cases}$$

gives after relaxation when $\varepsilon \rightarrow 0$

$$\mathbf{u} = \lambda \frac{h^2}{3} - \varepsilon \frac{h}{3} Re \left(-h^2 \operatorname{div} \left(\lambda \frac{h^3}{3} \right) + \operatorname{div} \left(h \lambda \frac{h^2}{3} \otimes \lambda \frac{h^2}{3} \right) + \nabla P + \operatorname{div}(\nabla h \otimes \nabla_{\mathbf{p}} E) - \nabla(h \operatorname{div}(\nabla_{\mathbf{p}} E)) \right)$$

and

$$\partial_t h + \operatorname{div}(h\mathbf{u}) = 0.$$

6 Appendix

In this section, we present the Proof of Lemma 2.1.

Part i) and iii) *Equation satisfied by \mathbf{v} .* Let us first recall that $\mathbf{v} = \alpha(q^2)\sqrt{\frac{\sigma(h)}{h}}\nabla h$ and therefore

$$h\mathbf{v} = \alpha(q^2)\sqrt{\sigma(h)}h^{3/2}\frac{\nabla h}{h} := \alpha(q^2)G(h)\mathbf{a},$$

with $G(h) = \sqrt{\sigma(h)}h^{3/2}$ and $\mathbf{a} = \nabla(\log(h))$. In order to write an evolution equation on $h\mathbf{v}$, the first step is to calculate evolution equations on \mathbf{a} , $G(h)$ and $\alpha(q^2)$. For that purpose, we consider the mass conservation law written as

$$\partial_t h + \mathbf{u}^t \nabla h + h \operatorname{div}(\mathbf{u}) = 0. \quad (36)$$

By dividing (36) by h and differentiating with respect to $x_i, i = 1, 2$, one finds

$$\partial_t \mathbf{a} + \nabla(\mathbf{u}^t \mathbf{a}) + \nabla(\operatorname{div}(\mathbf{u})) = 0. \quad (37)$$

By multiplying (36) by $G'(h)$, one finds

$$\partial_t G(h) + \mathbf{u}^t \nabla G(h) = -hG'(h) \operatorname{div}(\mathbf{u}), \quad G'(h) = \frac{\sigma'(h)h^{3/2}}{2\sqrt{\sigma(h)}} + \frac{3}{2}\sqrt{\sigma(h)h}. \quad (38)$$

From (36), we find that ∇h satisfies

$$\partial_t \nabla h + (\mathbf{u}^t \nabla) \nabla h = -\operatorname{div}(h \nabla \mathbf{u}^t) - \nabla h \operatorname{div} \mathbf{u}. \quad (39)$$

The derivatives of $q = \|\nabla h\|$ are given by

$$q \partial_t q = (\nabla h)^t \partial_t \nabla h, \quad q \partial_i q = (\nabla h)^t \partial_i \nabla h, \quad i = 1, 2.$$

This allows to calculate the equation on $\alpha(q^2)$. Indeed, we can write:

$$\begin{aligned} \partial_t \alpha(q^2) + \mathbf{u}^t \nabla \alpha(q^2) &= \alpha'(q^2) (\partial_t q^2 + (\mathbf{u}^t \nabla) q^2) \\ &= 2\alpha'(q^2) (\nabla h)^t (\partial_t \nabla h + (\mathbf{u}^t \nabla) \nabla h) \end{aligned}$$

By substituting the value of $\partial_t \nabla h$ given by (39) into the former equation, one finds

$$\partial_t \alpha(q^2) + \mathbf{u}^t \nabla \alpha(q^2) = -2\alpha'(q^2) ((\nabla h)^t \operatorname{div}(h \nabla \mathbf{u}^t) + q^2 \operatorname{div} \mathbf{u}). \quad (40)$$

Finally, by using the fact that $h\mathbf{v} = \alpha(q^2)G(h)\mathbf{a}$, one finds that the advective term $\operatorname{div}(h\mathbf{v} \otimes \mathbf{u})$ is given by

$$\operatorname{div}(\alpha(q^2)G(h)\mathbf{a} \otimes \mathbf{u}) = \alpha(q^2)G(h) ((\mathbf{u}^t \nabla) \mathbf{a} + \operatorname{div}(\mathbf{u}) \mathbf{a}) + ((\mathbf{u}^t \nabla)(\alpha(q^2)G(h))) \mathbf{a}.$$

We can now calculate the equation satisfied by \mathbf{v} using formula (37)–(40). More precisely we have

$$\begin{aligned} \partial_t(h\mathbf{v}) + \operatorname{div}(h\mathbf{v} \otimes \mathbf{u}) &= \partial_t(\alpha(q^2)G(h)\mathbf{a}) + \operatorname{div}(\alpha(q^2)G(h)\mathbf{a} \otimes \mathbf{u}) \\ &= \alpha(q^2)G(h) ((\partial_t + \mathbf{u}^t \nabla) \mathbf{a} + \operatorname{div}(\mathbf{u}) \mathbf{a}) + ((\partial_t + \mathbf{u}^t \nabla)(\alpha(q^2)G(h))) \mathbf{a} \\ &= \alpha(q^2)G(h) ((\mathbf{u}^t \nabla) \mathbf{a} + \operatorname{div}(\mathbf{u}) \mathbf{a} - \nabla(\mathbf{u}^t \mathbf{a} + \operatorname{div}(\mathbf{u}))) \\ &\quad - (\alpha(q^2)hG'(h) \operatorname{div}(\mathbf{u}) + 2G(h)\alpha'(q^2)((\nabla h)^t \operatorname{div}(h \nabla \mathbf{u}^t) + \operatorname{div}(\mathbf{u})q^2)) \mathbf{a} \\ &= \alpha(q^2)G(h) ((\mathbf{u}^t \nabla) \mathbf{a} - \nabla(\mathbf{u}^t \mathbf{a} + \operatorname{div}(\mathbf{u}))) \\ &\quad - \left(\left(\frac{hG'(h)}{G(h)} - 1 \right) \operatorname{div}(\mathbf{u}) + \frac{2\alpha'(q^2)}{\alpha(q^2)} ((\nabla h)^t \operatorname{div}(h \nabla \mathbf{u}^t) + \operatorname{div}(\mathbf{u})q^2) \right) h\mathbf{v}. \end{aligned}$$

Note that we have the relation

$$\alpha(q^2)G(h) \left((\mathbf{u}^t \nabla) \mathbf{a} - \nabla(\mathbf{u}^t \mathbf{a} + \operatorname{div}(\mathbf{u})) \right) = -\frac{\alpha(q^2)G(h)}{h} \operatorname{div}(h \nabla \mathbf{u}^t)$$

and therefore, by using the relation $h \mathbf{v} = \alpha(q^2) G(h) \mathbf{a}$, one finds

$$\begin{aligned} \partial_t(h\mathbf{v}) + \operatorname{div}(h\mathbf{v} \otimes \mathbf{u}) &= -\operatorname{div}(\mathbf{u}) \left(\frac{hG'(h)}{G(h)} - 1 + \frac{2\alpha'(q^2)q^2}{\alpha(q^2)} \right) h\mathbf{v} \\ &\quad - \frac{2\alpha'(q^2)}{\alpha(q^2)} \left(\frac{h^2 \mathbf{v}}{\alpha(q^2)G(h)} \right)^t \operatorname{div}(h \nabla \mathbf{u}^t) h\mathbf{v} - \frac{\alpha(q^2)G(h)}{h} \operatorname{div}(h \nabla \mathbf{u}^t). \\ &= -\operatorname{div}(\mathbf{u}) \left(\frac{hG'(h)}{G(h)} - 1 + \frac{2\alpha'(q^2)q^2}{\alpha(q^2)} \right) h\mathbf{v} \\ &\quad - \left(\frac{2\alpha'(q^2)}{\alpha(q^2)^2} \frac{h^3}{G(h)} \mathbf{v} \otimes \mathbf{v} + \frac{\alpha(q^2)G(h)}{h} I_d \right) \operatorname{div}(h \nabla \mathbf{u}^t). \end{aligned}$$

This yields the conclusion on the evolution of $h\mathbf{v}$.

Equation satisfied by \mathbf{u} . Let us first note that

$$\mathbf{p} = \frac{\mathbf{v}}{\alpha(q^2) \sqrt{\frac{\sigma(h)}{h}}}$$

and therefore

$$\nabla_{\mathbf{p}} E = \sigma(h) (\alpha(q^2)^2 + 2\alpha(q^2)\alpha'(q^2)\|\mathbf{p}\|^2) \mathbf{p} = \sqrt{\sigma(h)}\sqrt{h} (\alpha(q^2) + 2\alpha'(q^2)q^2) \mathbf{v}$$

Next, we expand $f(h, \mathbf{v})\mathbf{v}$ and $g(h, \mathbf{v}) \cdot \mathbf{v}$. First, one has

$$f(h, \mathbf{v})\mathbf{v} = \sqrt{\sigma(h)}\sqrt{h} \left(2\frac{\alpha'(q^2)h}{\alpha(q^2)^2\sigma(h)} \|\mathbf{v}\|^2 + \alpha(q^2) \right) \mathbf{v} = \sqrt{\sigma(h)}\sqrt{h} (2\alpha'q^2 + \alpha) \mathbf{v} = \nabla_{\mathbf{p}} E.$$

Now we observe that

$$\mathbf{p} \cdot \nabla_{\mathbf{p}} E = (2\alpha'(q^2)q^2 + \alpha(q^2)) \alpha(q^2)q^2\sigma(h).$$

This yields

$$\begin{aligned} \mathbf{g}(h, \mathbf{v}) \cdot \mathbf{v} &= \left(\left(\frac{\sigma'(h)h}{2\sigma(h)} + \frac{1}{2} \right) + 2\frac{\alpha'(q^2)}{\alpha(q^2)} q^2 \right) h \|\mathbf{v}\|^2 \\ &= \left(\left(\frac{\sigma'(h)h}{2\sigma(h)} + \frac{1}{2} \right) \alpha(q^2) + 2\alpha'(q^2)q^2 \right) \alpha(q^2)q^2\sigma(h) \\ &= (2\alpha'(q^2)q^2 + \alpha(q^2)) \alpha(q^2)q^2\sigma(h) - \left(1 - \frac{\sigma'(h)h}{\sigma(h)} \right) \frac{1}{2} (\alpha(q^2))^2 q^2 \sigma(h) \end{aligned}$$

and thus

$$\mathbf{g}(h, \mathbf{v}) \cdot \mathbf{v} = \mathbf{p}^t \nabla_{\mathbf{p}} E - (\sigma(h) - h\sigma'(h)) \mathcal{E}_{\text{cap}}(q).$$

Note that the momentum conservation equation of (2) can be written as:

$$\partial_t(h\mathbf{u}) + \operatorname{div}(h\mathbf{u} \otimes \mathbf{u}) + \nabla\pi = -\operatorname{div}(\nabla h \otimes \nabla_{\mathbf{p}} E) + \nabla(h \operatorname{div}(\nabla_{\mathbf{p}} E)) + \nabla((\sigma(h) - h\sigma'(h)) \mathcal{E}_{\text{cap}}(\|\nabla h\|)).$$

We now remark that

$$\operatorname{div}(h \nabla(f(h, \mathbf{v})\mathbf{v})^t) - \nabla(\mathbf{g}(h, \mathbf{v}) \cdot \mathbf{v}) = \operatorname{div}(h \nabla(\nabla_{\mathbf{p}} E)^t) - \nabla(\mathbf{p}^t \nabla_{\mathbf{p}} E - (\sigma(h) - h\sigma'(h)) \mathcal{E}_{\text{cap}}(q)).$$

Then, by taking $\mathbf{p} = \nabla h$, we obtain

$$\begin{aligned} \operatorname{div}(h\nabla(\nabla_{\mathbf{p}}E)^t) - \nabla(\mathbf{p}^t\nabla_{\mathbf{p}}E) &= \operatorname{div}(h\nabla(\nabla_{\mathbf{p}}E)^t) - \nabla((\nabla h)^t\nabla_{\mathbf{p}}E) \\ &= -\operatorname{div}(\nabla h \otimes \nabla_{\mathbf{p}}E) + \nabla(h\operatorname{div}(\nabla_{\mathbf{p}}E)) \end{aligned}$$

and consequently the right-hand side of the momentum equation in the augmented system is :

$$\operatorname{div}(h\nabla(f(h, \mathbf{v})\mathbf{v})^t) - \nabla(\mathbf{g}(h, \mathbf{v})^t\mathbf{v}) = -\operatorname{div}(\nabla h \otimes \nabla_{\mathbf{p}}E) + \nabla(h\operatorname{div}(\nabla_{\mathbf{p}}E)) + \nabla((\sigma(h) - h\sigma'(h))\mathcal{E}_{\text{cap}}(\|\nabla h\|))$$

and the momentum equation in the original system is satisfied, which gives the conclusion on \mathbf{u} for i).

Note that if (h, \mathbf{u}) is regular enough and the initial velocity \mathbf{v}_0 satisfies

$$\mathbf{v}_0 = \alpha(\|\nabla h_0\|^2) \sqrt{\frac{\sigma(h_0)}{h_0}} \nabla h_0$$

then \mathbf{v} satisfies also (8) and (h, \mathbf{u}) solves the original system.

Part ii). Recall that

$$E_{\text{tot}}(\mathbf{U}) = \frac{1}{2h} \left(\|h\mathbf{u}\|^2 + \|h\mathbf{v}\|^2 \right) + \Phi(h)$$

where \mathbf{U} is given by (9) and

$$\left(\frac{\Phi}{h} \right)' = \frac{\pi}{h^2}.$$

Let us consider the augmented system written as

$$\partial_t \mathbf{U} + \operatorname{div}(\mathcal{F}(\mathbf{U})) = \mathbf{M} \tag{41}$$

with the first order part given by

$$\mathbf{U} = \begin{pmatrix} h \\ h\mathbf{u} \\ h\mathbf{v} \end{pmatrix}, \quad \mathcal{F}(\mathbf{U}) = \begin{pmatrix} h\mathbf{u} \\ h\mathbf{u} \otimes \mathbf{u} + \pi(h)I_d \\ h\mathbf{v} \otimes \mathbf{u} \end{pmatrix}$$

whereas the capillary term on the right hand side of (41) is given by

$$\mathbf{M} = \begin{pmatrix} 0 \\ \operatorname{div}(h\nabla(f(h, \mathbf{v})\mathbf{v})^t) - \nabla(\mathbf{g}(h, \mathbf{v})^t\mathbf{v}) \\ -f(h, \mathbf{v})\operatorname{div}(h\nabla\mathbf{u}^t) \quad -\mathbf{g}(h, \mathbf{v})\operatorname{div}\mathbf{u} \end{pmatrix}.$$

Note that the left-hand side of (41) is conservative and hyperbolic and the right-hand side is skew-symmetric for the L^2 scalar product. This properties is real important to allow an appropriate splitting method which preserve the energy conservation at the discrete level.

The entropy variable \mathbf{V} for the first order part of (41) is given by

$$\mathbf{V}^t = (\nabla_{\mathbf{U}} E_{\text{tot}})^t = \left(-\frac{1}{2} \left(\|\mathbf{u}\|^2 + \|\mathbf{v}\|^2 \right) + \Phi'(h), \mathbf{u}^t, \mathbf{v}^t \right).$$

The energy equation is thus

$$\begin{aligned} \partial_t E_{\text{tot}} + \operatorname{div}(\mathbf{u}(E_{\text{tot}} + \pi)) &= (\nabla_{\mathbf{U}} E_{\text{tot}})^t \mathcal{M} \\ &= \mathbf{u}^t \operatorname{div}(h\nabla(f(h, \mathbf{v})\mathbf{v})^t) - \mathbf{u}^t \nabla(\mathbf{g}(h, \mathbf{v})^t\mathbf{v}) \\ &\quad - \mathbf{v}^t f(h, \mathbf{v}) \operatorname{div}(h\nabla\mathbf{u}^t) - \mathbf{v}^t \mathbf{g}(h, \mathbf{v}) \operatorname{div}(\mathbf{u}) \\ &= \mathbf{u}^t \operatorname{div}(h\nabla(f(h, \mathbf{v})\mathbf{v})^t) - (f(h, \mathbf{v})\mathbf{v})^t \operatorname{div}(h\nabla\mathbf{u}^t) \\ &\quad - \operatorname{div}(\mathbf{u}\mathbf{g}(h, \mathbf{v})^t\mathbf{v}) \\ &= \operatorname{div}(h(\mathbf{u}^t \nabla)(f(h, \mathbf{v})\mathbf{v})) - \operatorname{div}(h((f(h, \mathbf{v})\mathbf{v})^t \nabla)\mathbf{u}) - \operatorname{div}(\mathbf{u}\mathbf{g}(h, \mathbf{v})^t\mathbf{v}). \end{aligned}$$

Recall that $f(h, \mathbf{v}) \cdot \mathbf{v} = \nabla_{\mathbf{p}} E_{tot}$ and $\mathbf{g}(h, \mathbf{v}) \cdot \mathbf{v} = \mathbf{p}^t \nabla_{\mathbf{p}} E_{tot} - (\sigma - h\sigma') \mathcal{E}_{cap}(q)$ and therefore

$$\begin{aligned} \partial_t (E_{tot}) + \operatorname{div}(\mathbf{u}(E_{tot} + \pi)) &= (\operatorname{div}(h(\mathbf{u}^t \nabla)(\nabla_{\mathbf{p}} E_{tot})) - \operatorname{div}(h(\nabla_{\mathbf{p}} E_{tot}^t \nabla) \mathbf{u})) \\ &\quad - \operatorname{div}(\mathbf{u}(\mathbf{p}^t \nabla_{\mathbf{p}} E_{tot} - (\sigma - h\sigma') \mathcal{E}_{cap})). \end{aligned}$$

By choosing $\mathbf{p} = \nabla h$, we easily verify that

$$\begin{aligned} &(\operatorname{div}(h(\mathbf{u}^t \nabla)(\nabla_{\mathbf{p}} E_{tot})) - \operatorname{div}(h(\nabla_{\mathbf{p}} E_{tot}^t \nabla) \mathbf{u})) - \operatorname{div}(\mathbf{u} \mathbf{p}^t \nabla_{\mathbf{p}} E_{tot}) \\ &= (\operatorname{div}(h(\mathbf{u}^t \nabla)(\nabla_{\mathbf{p}} E_{tot})) - \operatorname{div}(h(\nabla_{\mathbf{p}} E_{tot}^t \nabla) \mathbf{u})) - \operatorname{div}(\mathbf{u}(\nabla h)^t \nabla_{\mathbf{p}} E_{tot}) \\ &= \operatorname{div}(h \operatorname{div}(\nabla_{\mathbf{p}} E_{tot}) \mathbf{u}) - \operatorname{div}(\operatorname{div}(h \mathbf{u}) \nabla_{\mathbf{p}} E_{tot}). \end{aligned}$$

Then we get

$$\partial_t (E_{tot}) + \operatorname{div}(\mathbf{u}(E_{tot} + \pi - (\sigma - h\sigma') \mathcal{E}_{cap})) = \operatorname{div}(h \operatorname{div}(\nabla_{\mathbf{p}} E_{tot}) \mathbf{u}) - \operatorname{div}(\operatorname{div}(h \mathbf{u}) \nabla_{\mathbf{p}} E_{tot})$$

which is exactly the formulation (6) of the Energy balance of the original system.

References

- [1] L. AGÉLAS, D. A. DI PIETRO, R. EYMARD, R. MASSON. An abstract analysis framework for non-conforming approximations of diffusion problems on general meshes. *Int. J. Finite Volumes*, 7(1):1–29, 2010.
- [2] S. BLAISE AND A. ST-CYR. A dynamic hp-adaptive discontinuous Galerkin method for shallow-water flows on the sphere with application to a global tsunami simulation. *Monthly Weather Review*, 140(3):978–996, 2012.
- [3] D. BRESCH, F. COUDERC, P. NOBLE, J.-P VILA. A generalization of the quantum Bohm identity: Hyperbolic CFL condition for Euler-Korteweg equations. *C.R. Acad. Sciences Paris* Volume 354, Issue 1, 39–43, (2016).
- [4] D. BRESCH, N. CELLIER, F. COUDERC, M. GISCLON, J. LALLEMENT, P. NOBLE, G. RICHARD, C. RUYER-QUIL, J.-P. VILA, P. VILLEDIEU. Triple points simulation in two-dimension using a generalized augmented system. In preparation (2019).
- [5] D. BRESCH, M. GISCLON, I. LACROIX-VIOLET. On Navier-Stokes-Korteweg and Euler-Korteweg systems: Application to Quantum Fluid Models. *Arch. Rational Mech. Anal.*, Vol. 233, Issue 3, 975–1025, (2019).
- [6] P. CASAL, H. GOUIN. Equations du mouvement des fluides thermocapillaires. *C. R. Acad. Sci. Paris, t. 306, Série II*, p. 99-104, (1988).
- [7] J. CAPECELATRO. A purely Lagrangian method for simulating the shallow water equations on a sphere using smooth particle hydrodynamics. *Journal of Computational Physics*, 356:174–191, 2018.
- [8] F. DHAOUDI, N. FAVRIE, S. GAVRILYUK Extended lagrangian approach for the defocusing non-linear Schrödinger equation. *Studies in Appl. Maths* (2019).
- [9] E. J. DOEDEL, T. F. FAIRGRIEVE, B. SANDSTED, A. R. CHAMPNEYS, Y. A. KUZNETSOV, X. WANG, AUTO-07P: Continuation and bifurcation software for ordinary differential equations, *Technical report* (2007).
- [10] C. ESKILSSON AND S.J SHERWIN. A triangular spectral/hp discontinuous Galerkin method for modelling 2D shallow water equations. *International Journal for Numerical Methods in Fluids*, 45(6):605–623, 2004.

- [11] J. FRANK AND S. REICH. The Hamiltonian particle-mesh method for the spherical shallow water equations. *Atmospheric Science Letters*, 5(5):89–95, 2004.
- [12] S. GAVRILYUK, H. GOUIN Symmetric form of governing equations for capillary fluids Trends in Applications of Mathematics to Mechanics. Eds. G. Iooss, O. Gués, A. Nouri. Monographs and Surveys in Pure and Applied Maths. Chapman & al 2000.
- [13] F.X. GIRALDO. Lagrange–Galerkin methods on spherical geodesic grids: the shallow water equations. *Journal of Computational Physics*, 160(1):336–368, 2000.
- [14] F.X. GIRALDO. A spectral element shallow water model on spherical geodesic grids. *International Journal for Numerical Methods in Fluids*, 35(8):869–901, 2001.
- [15] F.X. GIRALDO, J.S. HESTHAVEN, AND T. WARBURTON. Nodal high-order discontinuous Galerkin methods for the spherical shallow water equations. *Journal of Computational Physics*, 181(2): 499–525, 2002.
- [16] F.X. GIRALDO AND TIMOTHY WARBURTON. A nodal triangle-based spectral element method for the shallow water equations on the sphere. *Journal of Computational Physics*, 207(1):129–150, 2005.
- [17] H. GOUIN Symmetric forms for hyperbolic-parabolic systems of multi-gradient fluids. *Z Angew Math Mech* (2019).
- [18] R.S. JOHNSON. *A Modern Introduction to the Mathematical Theory of Water Waves*. Cambridge University Press, Cambridge, 1997.
- [19] G. R. JOHNSON, S. R. BEISSEL. Normalized smoothing functions for SPH +impact computations Internat. *J. Numer. Methods Engrg.*, 39 (1996), pp. 2725–2741.
- [20] D. J. KORTEWEG. Sur la forme que prennent les équations du mouvement des fluides si l’on tient compte des forces capillaires causées par des variations de densité considérables mais continues et sur la théorie de la capillarité dans l’hypothèse d’une variation continue de la densité. *Archives Néerlandaises des sciences exactes et naturelles*. Ser 2, 6:1–24, 1901.
- [21] J. LALLEMENT. Modélisation et simulation numérique d’écoulements de films minces avec effet de mouillage partiel. PhD Thesis 2019, ISAE Toulouse.
- [22] J. LALLEMENT, P. TRONTIN, C. LAURENT, P. VILLEDIEU. A shallow water type model to describe the dynamic of thin partially wetting films for the simulation of anti-icing systems. AIAA AVIATION Forum June 25-29, 2018, Atlanta, Georgia. 2018 Atmospheric and Space Environments Conference.
- [23] N. LANSON, J. P. VILA, Renormalized meshfree schemes I: Consistency, stability, and hybrid methods for conservation laws, *SIAM J. Numer. Anal.*, 46 (2008), pp. 1912–1934.
- [24] P. NOBLE, J.–P. VILA. Stability theory for difference approximations of Euler-Korteweg Equations and application to thin film flows. *SIAM J. Numerical Analysis*, 52, 6, 2770-2791, (2016).
- [25] S. POPINET. Numerical models of surface tension. *Annual Review of Fluid Mechanics*. Vol. 50, 49–75, (2018).
- [26] RAMACHANDRAN D NAIR, STEPHEN J THOMAS, AND RICHARD D LOFT. A discontinuous galerkin global shallow water model. *Monthly weather review*, 133(4):876–888, 2005.
- [27] G.L. RICHARD, M. GISCLON, C. RUYER-QUIL, J.–P. VILA. Optimization of consistent two-equation models for thin film flows. *European Journal of Mechanics / B Fluids* 76 (2019) 7–25.
- [28] G.L. RICHARD, C. RUYER-QUIL, J.P. VILA, A three-equation model for thin films down an inclined plane, *J. Fluid Mech.* 804 (2016) 162–200.
- [29] D. SERRE. Sur le principe variationnel des équations de la mécanique des fluides parfaits. *RAIRO – Modélisation mathématique et analyse numérique*, tome 27, no 6 (1993), p. 739-758

- [30] Y. XING, X. ZHANG, AND C.W. SHU. Positivity-preserving high order well-balanced discontinuous Galerkin methods for the shallow water equations. *Advances in Water Resources*, 33(12):1476–1493, 2010.

Acknowledgments. D. Bresch, M. Gisclon, N. Cellier and C. Ruyer-Quil have been supported by the Fraise project, grant ANR-16-CE06-0011 of the French National Research Agency (ANR) and with G.-L. Richard by the project Optiwind through Horizon 2020/Clean Sky2 (call H2020-CS2-CFP06-2017-01) with Saint-Gobain. This work was granted access to the HPC resources of CALMIP supercomputing center under the allocation 2019-P1234.

Authors coordinates: D. BRESCH, M. GISCLON, G.-L. RICHARD, LAMA UMR5127 CNRS, Université Savoie Mont-Blanc, 73376 Le Bourget du Lac, France.

Emails: didier.bresch@univ-smb.fr, marguerite.gisclon@univ-smb.fr, gael.loic.richard@orange.fr

N. CELLIER AND C. RUYER-QUIL, LOCIE UMR5271 CNRS, Université Savoie Mont-Blanc, 73376 Le Bourget du Lac, France.

Emails: contact@nicolas-cellier.net, christian.ruyer-quil@univ-smb.fr

F. COUDERC, P. NOBLE AND J.P. VILA. Institut de Mathématiques de Toulouse, UMR5219 CNRS, INSA de Toulouse, 31077 Toulouse cedex 4, France.

Emails: couderc@math.univ-toulouse.fr, pascal.noble@math.univ-toulouse.fr, vila@insa-toulouse.fr